

國立交通大學

光電工程研究所

碩士論文

以聚乙二醇為添加物製作高效能負型有機薄膜電晶體



**High-Performance n-channel organic thin-film
transistors incorporating poly(ethylene glycol)**

研究生：蔡宗翰

指導教授：陳方中 博士

中華民國九十九年七月

以聚乙二醇為添加物製作高效能負型有機薄膜電晶體

High-Performance n-channel organic thin-film transistors incorporating poly(ethylene glycol)

研究生：蔡宗翰

Student : Tzung-Han Tsai

指導教授：陳方中 博士

Advisor : Dr. Fang-Chung Chen



A Thesis
Submitted to Institute of Electro-Optical Engineering
College of Electrical and Computer Engineering
National Chiao Tung University
In Partial Fulfillment of the Requirements
For the Degree of Master
In
Electro-Optical Engineering
July 2010
Hsinchu, Taiwan, Republic of China

中華民國九十九年七月

以聚乙二醇為添加物製作高效能負型有機薄膜電晶體

學生：蔡宗翰

指導教授：陳方中

國立交通大學光電工程研究所

中文摘要

本研究選用聚乙二醇，將其添加至負型[6,6]-phenyl C₆₁-butyric acid methyl ester (PCBM) 有機薄膜電晶體之主動層中，研究其對元件特性之影響。由實驗結果可知添加適當比例之高分子量聚乙二醇能夠有效的提高元件效能並且表現出較好的穩定性。在本研究中，加入聚乙二醇之元件載子遷移率可由 0.014 cm²/Vs 提升至 0.044 cm²/Vs，而臨界電壓也可由 17V 縮小至-2V。在大氣環境下量測，未添加聚乙二醇之元件載子遷移率變為原本之千分之一，而添加聚乙二醇後則為十分之一。這可歸功於聚乙二醇分子與鋁電極產生化學反應，進而減少電子注入障礙。

High-Performance n-channel organic thin-film transistors incorporating poly(ethylene glycol)

Student: Tzung-Han Tsai

Advisor: Dr. Fang-Chung Chen

Institute of Electro-Optical Engineering
National Chiao Tung University

Abstract

This study investigates the effect of blending of poly(ethylene glycol) (PEG) into the active layer on the performance of n-channel organic thin-film transistors (OTFTs) based on [6,6]-phenyl C₆₁-butyric acid methyl ester (PCBM). We found that the performance and the stability of the OTFTs could be enhanced after the addition of PEG. The mobility could be improved from 0.014 to 0.044 cm²/Vs, and the threshold voltage shifted from 17V toward to -2V. In the ambient conditions, the mobility of the pristine-PCBM device degraded by three orders. However, the one of the device prepared with PEG only decreased by one order. The enhancement could be attributed into the reduction of the electron injection barrier due to the chemical reactions between PEG molecules and Al atoms of the source/drain electrodes.

謝誌

這個世代的人在中學時期一定會上過這樣一堂國文課，那就是陳之藩的《謝天》，文中提到：「要謝的人太多了，就謝天吧。」但我想這也許是我一生中唯一一次有機會可以好好的謝謝大家，所以還是一一說起吧。

能走到今天這一步，最應該要感謝的，就是我的家人，從小到大，爸媽為了栽培我跟弟弟，省吃儉用，寧願自己用最差的，也要讓我們用最好的，小的時候，爸爸一年三百六十五天幾乎天天在工作，只為了讓我們有更好的生活，媽媽身體不好卻還是不顧健康的去擺攤，但當時年紀還小的我卻無力改變什麼，高中時貪玩荒廢課業，讓你們失望。現在不一樣了，你們的努力總算沒有白費，未來你們好好休息，這個家，換我來付出。

來實驗室的兩年，衷心感謝陳方中老師的指導，老師總是不保留的將自己所學以及經驗與大家分享，不管是在研究上或是處事方法，都使我有更深一層的見解，也因此思考一件事情時我也開始變的有條理，如何從零開始的完成一件事更是讓我終身受用。

再來要感謝博士班的學長 KOBE、志力、孝信、兆峰，我常會會問一些對你們來說很簡單的問題，但你們卻願意耐心地替我解答，讓我能順利的完成研究。畢業的學長姐們，阿寬、曾博、+0、POPO、達爾、小公主，謝謝你們在我碩一時的協助，一開始對這個領域完全沒概念的我，已經有了成長，和你們相處很愉快，碩士生活也因此有了更多樂趣。

最要感謝的就是同屆一起打拚的這一群人了，首先要感謝的就是浩智，感謝你總是願意放下自己手邊的事來幫我處理一些雜事，實驗上因為你聰明的頭腦，幫我解決了很多問題，且你總是願意配合我來娛樂大家，祝你一切順利。再來要感謝阿凱、阿達、洪毅，說起來我們是真正同屆的伙伴，從開始的不熟識直到現在已經要各奔東西，兩年來不管是在實驗或是生活上的互相協助都讓我感受到出外靠朋友的溫馨，未來有機會要多相聚。再來要感謝 500，不愧是有機電晶體一哥，跟你討論總能在你身上學到東西，重點是感謝你還帶我去打壘球，讓我在這兩年還能體會到在紅土場上奔馳的快感，希望還有機會一起打球。還有老薛感謝妳常關心我以及拿東西給我吃，未來也要一起加油。還有學弟紹棠、小白，你們適時的協助總是很重要，謝謝你們，你們也要順利畢業。

感謝這兩年來一起來到新竹一起努力的林 JJ 跟撲弟，在我難過低潮時總是與我一同分擔，我們總是分享彼此的好與壞，在中興的四年裡，一起玩，一起搞系學會，一起辦宿營，我們一起完成多少可以讓我們回味無窮的活動，也許未來這樣的機會已經很難得，希望認識六年的交情跟默契可以一直持續下去。感謝中興物理皇家系壘的所有人，也許我們總是差一個冠軍，但那些努力的過程絕對是最真實的。還要感謝烏烏、阿昌、石帥、益安、子欣、阿璇、郭品超、浩呆、阿竹、麟王彥、小尻、綠豆、小飛象、豆子、小劉…族繁不及備載，這六年來認識你們真好，能順利走到這裡，你們居功厥偉。還要感謝 SE，從國一一直到大四，從好友到情人，妳總是陪在我身旁，我們的過去將會是我一輩子最寶貴的回憶。可能還有很多沒提到的人，也謝謝你們。

最後感謝的人是 iihang，謝謝妳讓我找回積極，讓我知道我還能做什麼，這一年中妳的關心讓我渡過好多低潮，我們的未來還很長，一起走下去吧。

Contents

中文摘要	i
Abstract	ii
謝誌	iii
Contents	iv
List of Figures	vi
List of Tables	viii
Chapter 1	1
Introduction	1
1.1 Preface	1
1.2 Organic Thin-Film Transistors	3
1.2.1 Introduction to Organic Semiconductors	3
1.2.2 Overview of Organic Thin-Film Transistors	3
1.2.3 Overview of n-channel Organic Thin-Film Transistors	4
1.2.4 Introduction to the N-channel Material PCBM	6
1.3 Motivation	7
1.4 Thesis Organization	9
Chapter 2	10
Mechanism and Operation	10
2.1 Structures of Organic Thin Film Transistors	10
2.2 The Charge Carrier Transportation in Organic Semiconductors	11
2.2.1 Preface	11
2.2.2 Polaron and Bipolaron	12
2.2.3 Hopping Model	13
2.2.4 Multiple Trapping and Release Model (MTR)	14
2.3 The Operation of Organic Thin-Film Transistors	14
2.3.1 Energy Level Principle and Carrier Distribution	14
2.3.2 The Methods of Extracting Parameters	18
2.3.3 Contact resistance	20

Chapter 3.....	21
Experimental and Analysis Methods.....	21
3.1 Substrate Preparation.....	21
3.1.1 Preface	21
3.1.2 ITO Patterning Process.....	21
3.1.3 Cleaning of ITO/Glass Substrate.....	23
3.1.4 Cleaning of SiO₂/Si Substrate.....	23
3.2 The Materials.....	24
3.3 Device Fabrication Process of OTFTs.....	25
3.3.1 Spin-Coating Polymer Dielectric Film.....	25
3.3.2 Spin-Coating of PCBM/PEG Blends as the Active Layer and Evaporation of Metal Electrodes	25
3.4 Measurements and Analysis of OTFTs	28
3.4.1 Electrical Characteristics.....	28
3.4.2 Capacitance Analysis.....	28
3.4.3 Surface Morphology Measurement.....	28
3.4.4 X-ray Photoelectron Spectroscopy Measurement.....	30
Chapter 4.....	32
Results and Discussion.....	32
4.1 Characteristics of Device Electrical Properties	32
4.1.1 The Effect of Molecular Weight of PEG.....	32
4.1.2 The Effect of PEG Concentration.....	35
4.1.3 The Electrical Characteristics Measured in the Atmosphere.....	38
4.1.4 The Effect of PEG on the Devices Fabricated on PVP/SiO₂ Substrate	40
4.2 Morphological Analysis of the Active Films.....	43
4.3 Analysis of Device Resistances	45
4.4 The Analysis of XPS Measurements.....	48
Chapter 5.....	49
Conclusion and Future Work	49
5.1 Conclusion.....	49
5.2 Future Work.....	49
Reference.....	50

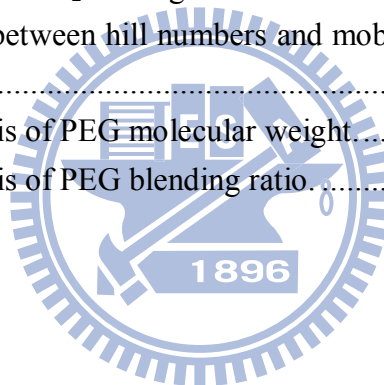
List of Figures

Figure 1.1	The application of organic electronics: a “rollable” OFET-driven OLED Display that can wrap around a pencil.....	2
Figure 1.2	The application of organic electronics: a transparent OLED Display.....	2
Figure 1.3	N-type organic semiconducting materials.	5
Figure 1.4	The chemical structure of [6,6]-phenyl C ₆₁ -butyric acid methyl ester (PCBM)...	6
Figure 1.5	Out-of-plane XRD pattern of spin-coated PCBM film.	7
Figure 2.1	Two TFT structures (a) Top contact (b) Bottom contact.	10
Figure 2.2	The structure of polarons.	12
Figure 2.3	The origin of polaron in energy band.....	13
Figure 2.4	Intermolecular charge carrier hopping.....	13
Figure 2.5	(a) The energy level diagram of an OTFT at $V_G = 0$ and $V_D = 0$. (b-e) the mechanism of OTFT operation for the case of electron (b) accumulation and (d) transport; hole (c) accumulation and (e) transport.	15
Figure 2.6	(a) Carrier concentration diagram of TFT in the linear regime. (b) Pinch-off occurs when $V_D \sim V_G - V_T$. (c) Carrier concentration diagram of TFT in the saturation regime	17
Figure 2.7	(a) $I_D - V_D$ curves for a n-OTFT for various V_G . (b) $I_D - V_G$ curves for various V_D , and the $I_D^{0.5} - V_G$ curve is shown on the right-handed axis.....	19
Figure 2.8	The illustration of transfer line method.	20
Figure 3.1	The process of ITO patterning.	22
Figure 3.2	The structure of organic materials used in this experiments.	24
Figure 3.3	The energy level diagram of the materials used in this study.	24
Figure 3.4	The flow chart of the device fabrication process (ITO/glass substrates).	26
Figure 3.5	The flow chart of the device fabrication process (Si/SiO ₂ substrates).	27
Figure 3.6	The interaction force between two atoms.	29
Figure 3.7	The operation method of AFM.	29
Figure 3.8	Basic components of monochromatic XPS system.....	31
Figure 3.9	XPS C1s spectra.	31

Figure 4.1 The I_D - V_D output curves of (a) pure PCBM device, and device prepared with PEG (b) 400, (c) 1000, (d) 3000, (e) 8000, and (f) 20000, respectively.	33
Figure 4.2 The (a) I_D - V_G and (b) $I_D^{1/2}$ - V_G transfer curves at $V_D = 60V$ with distinct molecular weight of PEG blending.	34
Figure 4.3 The I_D - V_D output curves of (a) pure PCBM OTFTs, and with (b) 1%, (c) 5%, (d) 8%, (e) 11%, and (f) 16% PEG 20000 blending, respectively.	36
Figure 4.4 The (a) I_D - V_G and (b) $I_D^{1/2}$ - V_G transfer curves at $V_D = 60V$ with distinct concentration of PEG 20000 blending.	37
Figure 4.5 The I_D - V_D output curves of the OTFTs (a) without and (b) with PEG 1500 (5%) blending in the ambient environment.	38
Figure 4.6 The (a) I_D - V_G and (b) $I_D^{1/2}$ - V_G transfer curves at $V_D = 30 V$ and $60 V$ of the OTFTs with and without PEG blending in ambient environment.	39
Figure 4.7 The I_D - V_D output curves of the OTFTs prepared (a) without, and (b) with PEG 400 on PVP/SiO ₂ substrates.	40
Figure 4.8 The (a) I_D - V_G and (b) $I_D^{1/2}$ - V_G transfer curves at $V_D = 60 V$ of the OTFTs with and without PEG blending on PVP/SiO ₂ substrates.	41
Figure 4.9 The height-mode images measured by AFM : (a) pristine PCBM, (b) to (f) PEG 400 (5%), PEG 1000 (5%), PEG 3000 (5%), PEG 8000 (5%), and PEG 20000 (5%), respectively.	44
Figure 4.10 Total resistance as a function of channel resistance at various gate voltages. (a) pristine-PCBM; (b) with PEG 20000 (5%).	45
Figure 4.11 The C1s XPS spectra of PCBM/Al with and without PEG.	48

List of Tables

Table 4.1	The parameters of the OTFTs with distinct PEG molecular weight (MW) blending measured in nitrogen filled glove box.....	34
Table 4.2	The parameters of the OTFTs with different ratio PEG 20000 blending measured in nitrogen filled glove box.....	37
Table 4.3	The comparison of transfer characteristics of the OTFTs measured in inert and ambient environment.....	38
Table 4.4	The parameters of the OTFTs prepared with and without PEG blending on PVP/SiO ₂ substrates.....	41
Table 4.5	The continuous measurement parameters of the pristine PCBM OTFT on PVP/SiO ₂ substrates in N ₂ -filled glove box.....	42
Table 4.6	The continuous measurement parameters of the PEG (5%) /PCBM OTFT on PVP/SiO ₂ substrates in N ₂ -filled glove box.....	42
Table 4.7	The relationship between hill numbers and mobility with distinct molecular weight (M.W.) of PEG.....	43
Table 4.8	Resistance analysis of PEG molecular weight.....	45
Table 4.9	Resistance analysis of PEG blending ratio.....	46



Chapter 1

Introduction

1.1 Preface

Over the last few years, the organic electronic devices such as organic light-emitting diodes (OLEDs), organic photovoltaic cells (OPVs), and organic field-effect transistors (OFETs) have received much attention [1, 4]. Because many of the organic or polymer molecules can be dissolved in organic solvents, the solution can be used for large-area fabrication, such as using spin-casting or ink-jet printing processes. Because the production process of organic electronics only requires relatively low temperature, usually less than 200 °C, plastics could be potentially used as the substrates. However, some problems still remain to be solved. The organic semiconductors are very unstable and sensitive to the environment; the mobility is also much lower than the typical values of inorganic semiconductors.

At Society for Information Display (SID)-2010 electronic-display exhibition in Seattle (May 23-May 28), Sony Corporation announced a flexible, 80 μm -thick, full color OLED display (4.1-inch) driving by OFETs which can be enveloped around a thin cylinder with a radius of 4 mm (Figure 1.1).

In the same conference, Samsung Mobile Display showed their 19-inch transparent AMOLED display. Its transparency is reported to be over 30%. It can deliver the usage in notebook, car windshields, and for storefront advertising. The prototype is shown in Figure 1.2.

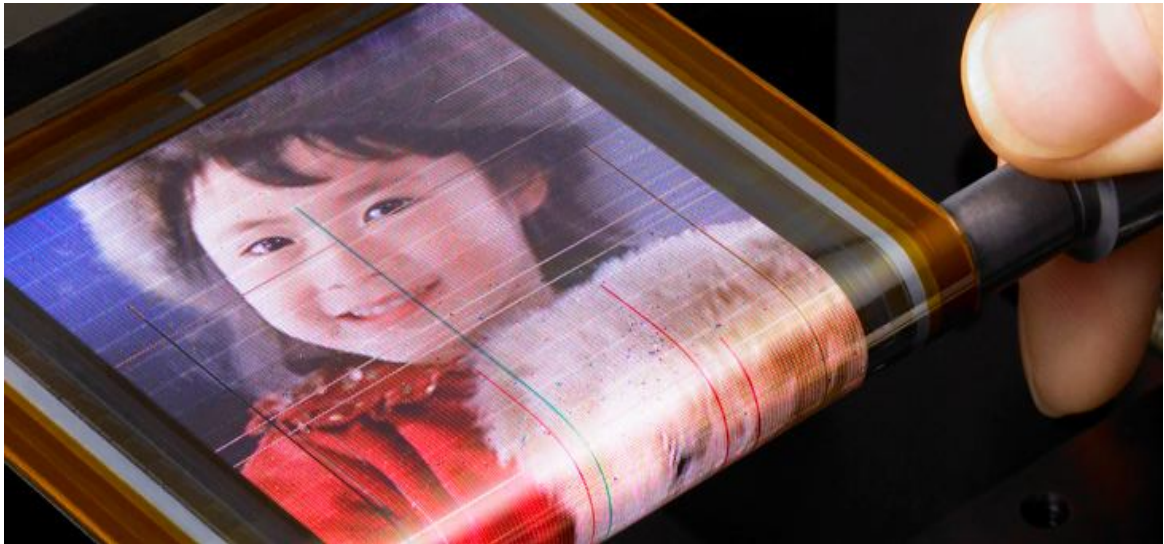


Figure1.1 The application of organic electronics: a “rollable” OFET-driven OLED Display that can wrap around a pencil. [Adapted from <http://en.akhilbarnews.com/47902/display>]



Figure1.2 The application of organic electronics: a transparent OLED Display. [Adapted from <http://en.akhilbarnews.com/47796/display>]

1.2 Organic Thin-Film Transistors

1.2.1 Introduction to Organic Semiconductors

Organic semiconductors are organic materials within semiconducting properties. We can classify them into two categories: oligomers and polymers. Oligomers consist few repeat units. Oligomers include dimers, trimers and tetramers. OTFTs fabricated from oligomers have been demonstrated with high mobilities (2-40 cm²/Vs) [7, 50].

Polymers are large molecules (macromolecule) which are composed of a long chain made of hydrogen and carbon elements. Bonding occurs when the carbon atoms are brought together. It forms the backbone of the molecule and leaves one weakly π -bonded electron. This π -bonded electron can transport in the polymer while an electric field is applied. Park *et al.* demonstrated the TFTs fabricated by the poly(3-hexylthiophene) polymer. They have relatively lower mobilities (0.04 cm²/Vs) [51].

The most important advantage of organic semiconductors is that they can be processed at lower temperatures, which means they are suitable for flexible plastic substrates. Many developers in this field have high interest in this subject, and try to improve the process techniques.

1.2.2 Overview of Organic Thin-Film Transistors

Organic thin-film transistors (OTFTs) have received much attention from many scientists. The first OTFT was demonstrated in 1983 by F. Ebisawa *et al* [2]. The authors used polyacetylene and polysiloxane as the active layer and the dielectrics, respectively in the devices. However, the mobility was just 1×10^{-5} cm²/Vs and the device did not show pinch-off. In past decade, organic thin-film transistors with improved performance have been reported. In 1997, Lin *et al.* demonstrated an OTFT, whose mobility was greater than 1 cm²/Vs for the first time [49]. In 2007, Takeda et al. proposed a very high-mobility OTFT which was

fabricated with single-crystal rubrene. The maximum mobility is evaluated as high as 40 cm^2/Vs [50].

1.2.3 Overview of n-channel Organic Thin-Film Transistors

So far, the electrical performances of p-channel organic OTFTs such like mobility and stability are much better than those n-channel devices. However, the n-channel OTFTs still play important roles in the production of electronics (ex: CMOS inverters). The common n-channel semiconductors are shown in Figure 1.3.

In general, the operation of many n-channel OTFTs is not stable in ambient conditions. It is attributed to its sensitivity to water and oxygen. The organic radical anions are produced in the channel as applying a positive gate voltage. These radical anions have a very high reducing power that can react effectively with water or oxygen. Hence most of n-channel OTFTs can only be measured and operated under inert environment such as in a nitrogen-filled glove box [16-18].

Besides, there are two major challenges that have to be overcome for improving the performance of n-channel OTFTs. First, the electrons are easily trapped by hydroxyl groups at the semiconductor-insulator interfaces. This problem can be solved by using hydroxyl-free polymer insulator materials [17, 31]. For example, a special kind of polyvinyl alcohols (Mowiol® 40-88) has been used as the gate insulator material and formed an electron-trap-free interface [31].

The second issue of enhancing the performance of n-channel OTFTs is their poor injection of electrons from the source/drain (S/D) electrodes into the semiconducting layer. For high-performance n-channel OTFTs, electrons need to inject efficiently into the lowest unoccupied molecular orbitals (LUMOs). The LUMO of the organic semiconductor usually locates at around 2 to 3 eV verse the vacuum energy level. Better electron injection can be

achieved by introducing low work function metals, such as Ca, Al, and Mg. However, all these metals are very unstable under ambient environmental. Cho *et al.* demonstrated n-channel OTFTs inserting titanium sub-oxide (TiO_x) at the electrodes/semiconductor interface [52]. This method can not only effectively improve the electron injection but also protect the channel from the influence of the environmental. Now for n-channel materials, the mobility up to $6 \text{ cm}^2/\text{Vs}$ has been improved using fullerene molecules made through vacuum evaporation as the active material [23, 24].

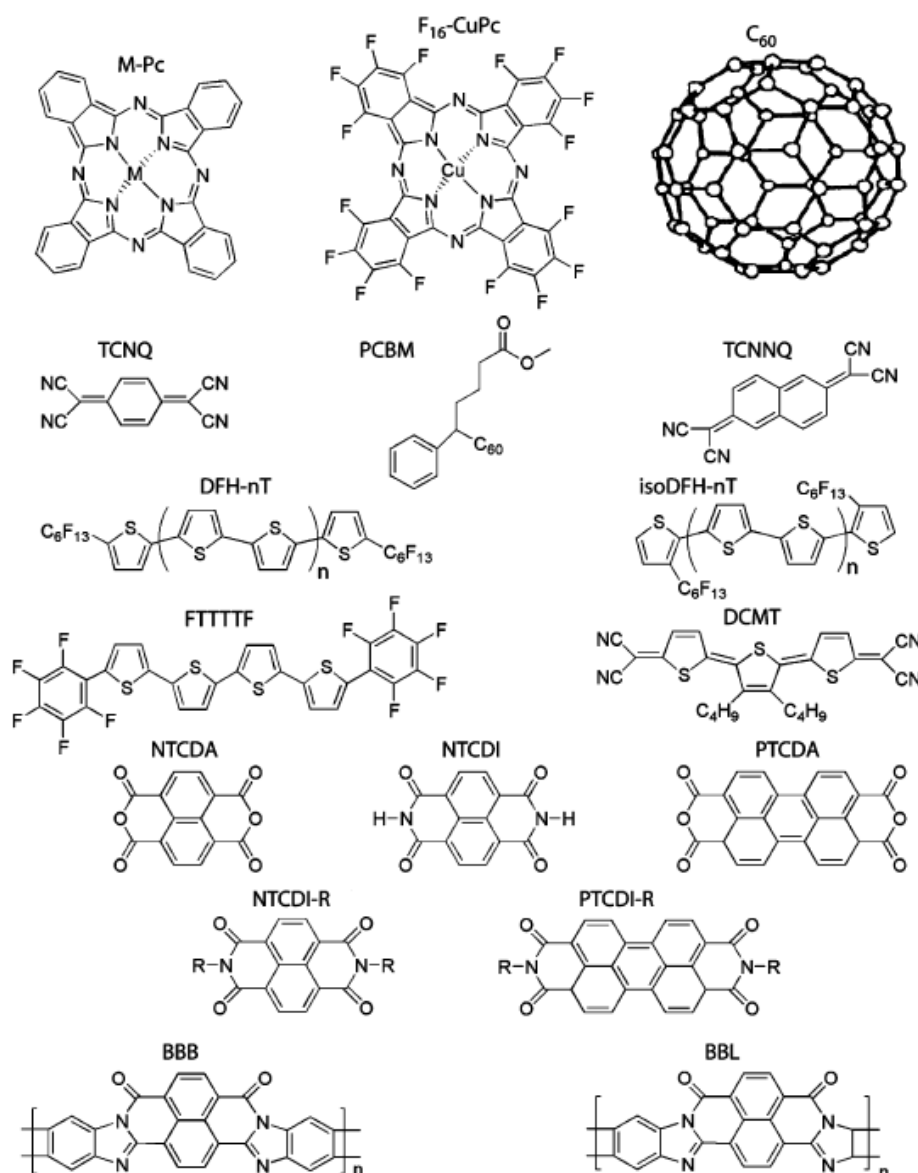


Figure1.3 N-type organic semiconducting materials [5].

1.2.4 Introduction to the N-channel Material PCBM

Fullerene molecules have a high electron affinity and have been widely used for fabrication of high-performance n-channel OTFTs [23, 24]. In this study, a fullerene derivative, [6,6]-phenyl C₆₁-butyric acid methyl ester (PCBM), has been chosen as the organic semiconductor. PCBM is solution-processable and its chemical structure is shown in Figure 1.4.

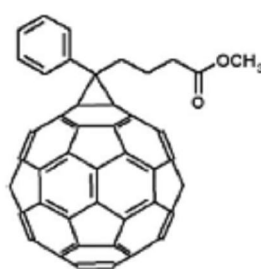


Figure 1. 4 The chemical structure of [6,6]-phenyl C₆₁-butyric acid methyl ester (PCBM) [22].

The highest occupied molecular orbital (HOMO) of PCBM is about -6.1 eV and the lowest unoccupied molecular orbital (LUMO) of PCBM is about -3.7 eV. Researchers have chosen PCBM as an electron acceptor and a conducting polymer, poly(3-hexylthiophene) (P3HT), as an electron donor to form the most successful model materials system for organic photovoltaic. Power conservation efficiencies of these bulk heterojunction polymer photovoltaic cells have been reported to be around 5%, and these devices also exhibited thermal stability [53].

Nevertheless, less attention has been paid to the morphology of pristine PCBM. In general, the spin-coated PCBM thin film forms disarranged structure [21]. No diffraction peaks and homogeneous morphology were observed in the PCBM thin film from the the results of X-ray diffraction (XRD) and the atomic force microscope (AFM) measurements

[20], which are shown in Figure 1.5.

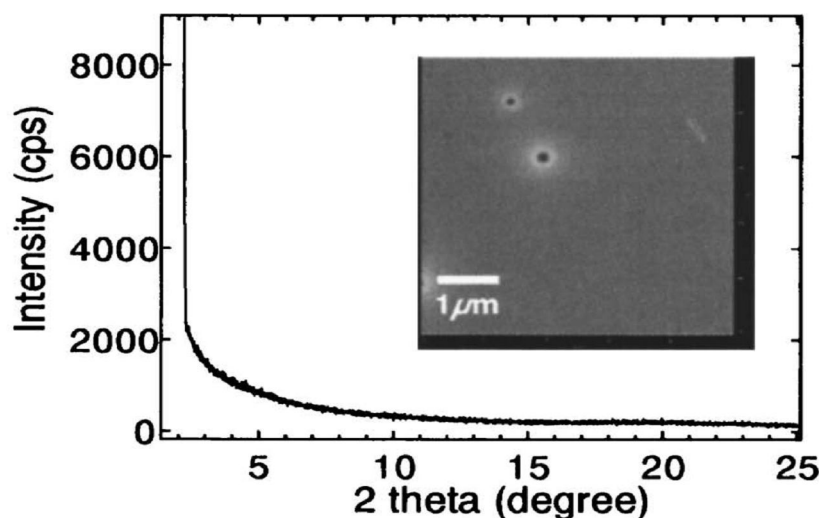


Figure 1.5 Out-of-plane XRD pattern of spin-coated PCBM film. Inset shows AFM image of PCBM film [20].

Recently, PCBM has showed its high performance with high electron mobility up to 0.03 -0.04 cm^2/Vs [22, 37]. It points that PCBM can act as a good semiconductor material for n-channel organic devices and as a building block for organic CMOS semiconductor circuits.

1.3 Motivation

In recent years, the highest mobility of n-channel Organic thin-film transistors (OTFTs) reported is up to $6\text{cm}^2/\text{Vs}$ for fullerene molecules by vacuum deposition [23, 24]. However, to take the advantages of low cost and easy processing, solution-processed OTFTs are needed. Mobility values from 0.18 to 0.9 cm^2/Vs are already obtained with high ON/OFF ratios for the solution-processed p-type materials [25-28], although the n-type solution-processed OTFTs are still lagging in performance.

The solution-processed fullerene derivatives are known as potential candidates for high-performance n-channel OTFTs [18-20, 29-31]. Higher electron mobility with

low-work-function calcium S/D electrodes were also reported [32], but these metals are easily oxidized and, therefore, the devices need further passivation.

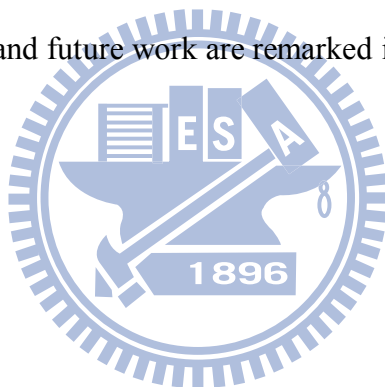
An alternative approach for replacing the reactive metals as an electrode is to insert a thin layer of alkali metal halides [33] or carboxylates [34], in various efforts for improving the charge injection from an Al cathode to an emitting layer for organic light emitting diodes (OLED). Similarly, the S/D contacts in the OTFTs have significant influence on device operation. For example, it has been reported that the electrical properties of n-channel OTFTs can be enhanced by inserting a nanoscale Cs_2CO_3 interfacial layer between the PCBM active layer and the S/D electrodes [37]. The presence of the Cs_2CO_3 layer at the organic/Al interface reduced the contact barriers and provided protection against diffusion and chemical interaction between the organic film and metal electrodes. But all the above-mentioned method needed many fabrication steps.

Vertical segregation between organic molecules and its application toward improving the performance of organic electronic devices have become topics of strong research activity [38-44]. To enhance the efficiency and increase the stability of polymer solar cells, Chen *et al.* introduced a nanoscale functional interlayer, containing poly(ethylene glycol) (PEG) through spontaneous vertical phase separation [44]. During the spin-coating process, the PEG molecules migrated to the surface and formed a thin layer on top of the active polymer layer without the need for any additional fabrication steps. After thermal deposition, the chemical interaction between the PEG monolayer and the Al atoms lowered the barrier height and contact resistance. As a result, the device performance has been improved.

Although high-performance devices made of solution-processed fullerene derivatives have been reported, most of them need additional fabrication steps to modify or protect the active layer. We try to develop a simple fabrication method that made the active thin-film containing poly(ethylene glycol), intend to achieve the same results in one step.

1.4 Thesis Organization

This thesis is organized as followings. In this chapter, the background of this study is described briefly; and in the following chapter, we have introduced the basic mechanism and device structures of organic field-effect transistors. The useful methods of analysis are also presented in this part. The experimental details are shown in the third chapter and the organization of OTFT is illustrated including substrate preparing and thin-film coating. Except for the device fabrication, the analysis methods are also particularly taken into consideration. In Chapter 4, there are discussions for devices prepared with and without blending poly(ethylene glycol) (PEG). Further, the role of PEG in the semiconducting layer is investigated by using atomic force microscope (AFM) and X-ray photoelectron spectroscopy (XPS). Finally, conclusions and future work are remarked in last chapter.



Chapter 2

Mechanism and Operation

2.1 Structures of Organic Thin Film Transistors

The conventional field-effect transistors (FETs) are based on the inorganic materials such as Si and Ge. The common FETs are metal-oxide-semiconductor field-effect transistors (MOSFETs). The MOSFETs are used extensively in digital circuits. Because of its relatively small size, millions of devices can be fabricated in a single integrated circuit (IC). The structures of thin-film transistors (TFTs) are similar to FETs, and the main difference is the thickness of active layer.

If we replace the inorganic semiconductor with organic semiconductor, the new device is called organic thin-film transistors (OTFTs). According to the order of depositing semiconducting materials, OTFTs are classified to two structures: top-contact (TC) and bottom-contact (BC). While the active layer is deposited first, and source and drain (S/D) electrodes are fabricated later, the structure is called TC. But the BC structure is opposite. The two different OTFTs structures are shown in Figure 2.1.

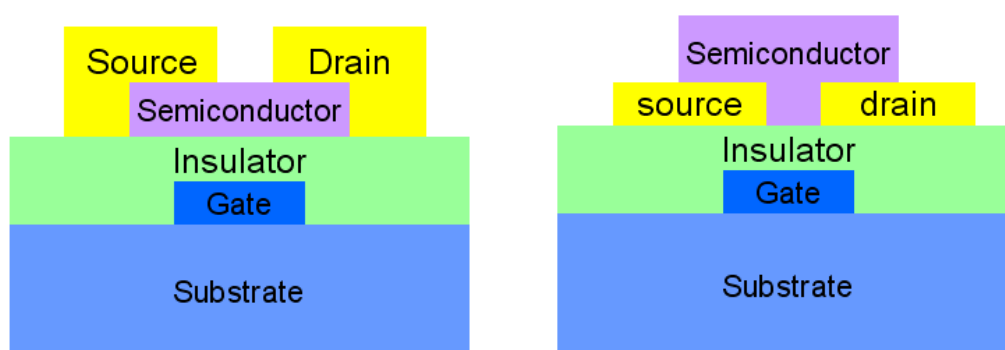


Figure 2.1 Two TFT structures (a) Top contact (b) Bottom contact.

General speaking, because of the poor adhesion of organic molecules on metal surface, it provides a bad growth base for the active layer. Therefore the device performances of TC OTFTs are better than BC OTFTs due to the small contact resistance at the semiconductor/electrodes interface. But the photolithography process cannot be used after depositing the active layer due to the damage of organic materials during the etching process. Hence we usually use the shadow mask to define the channel length, and the length scale is limited to 40 μm . We have to introduce BC structure to fabricate the smaller length device.

2.2 The Charge Carrier Transportation in Organic Semiconductors

2.2.1 Preface

The molecular interaction between organic semiconductors is different than inorganic semiconductors. They are covalent bonding and van der Waals force in inorganic and organic molecules, respectively. There are two distributions of π -bonding electrons in organic materials: localized states and delocalized states. The definition of localized states is that the electrons are bound to particularly atom. On the contrary, we can find some free electrons in π -bonding without direct relationships to specific atom, they are called delocalized states. The carriers in inorganic semiconductor materials are all delocalized states due to the extended bandgap. By the confinement in localized states, the mobility of organic semiconductor is relatively lower than that of inorganic semiconductor.

Up to now, the charge carrier transportation in organic semiconductors is still unobvious. There are three common models in organic semiconductors: polaron and bipolaron [8], hopping [54], and multiple trapping and release models [46].

2.2.2 Polaron and Bipolaron

The polaron is an electron or a hole in a conjugated molecule systems together with a cloud of phonons that is result from the deformation of the lattice produced by the interaction of the charges. The energy level is rearranged and the new one is defined as polaron energy level. The polaron structure is shown in Figure 2.2.

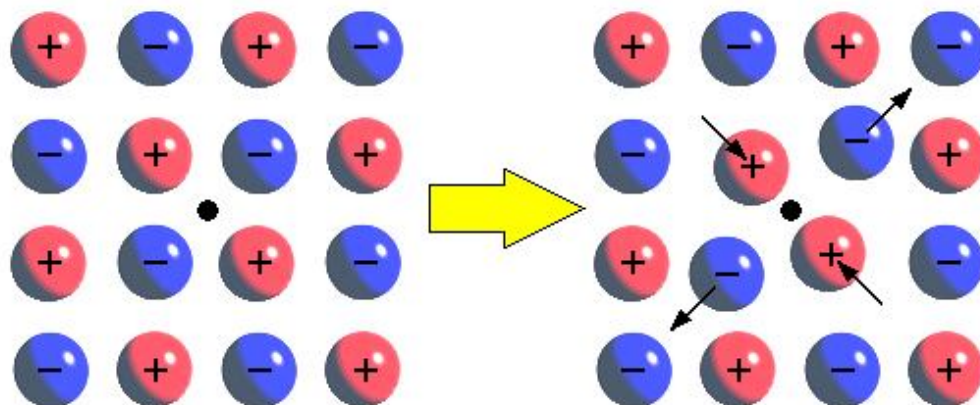


Figure 2.2 The structure of polarons. [Adapted from <http://upload.wikimedia.org/wikipedia/commons/d/d0/Polaron>]

When two polarons are close together, they can lower their energy by sharing the same deformations, which leads to an effective attraction between the polarons. If the interaction is sufficiently large, then the attraction leads to a bound bipolaron, thereby forming bipolaron energy levels. The origin of polaron in the energy band is shown in Figure 2.3.

If there are many bipolarons in conjugated molecules, the energy of carriers is overlapped near the edge of energy bands as highly doping in organic semiconductors, and the narrow bipolaron bands is formed between LUMO and HOMO levels. If we apply an external electric field, the polarons and bipolarons can move in the energy band.

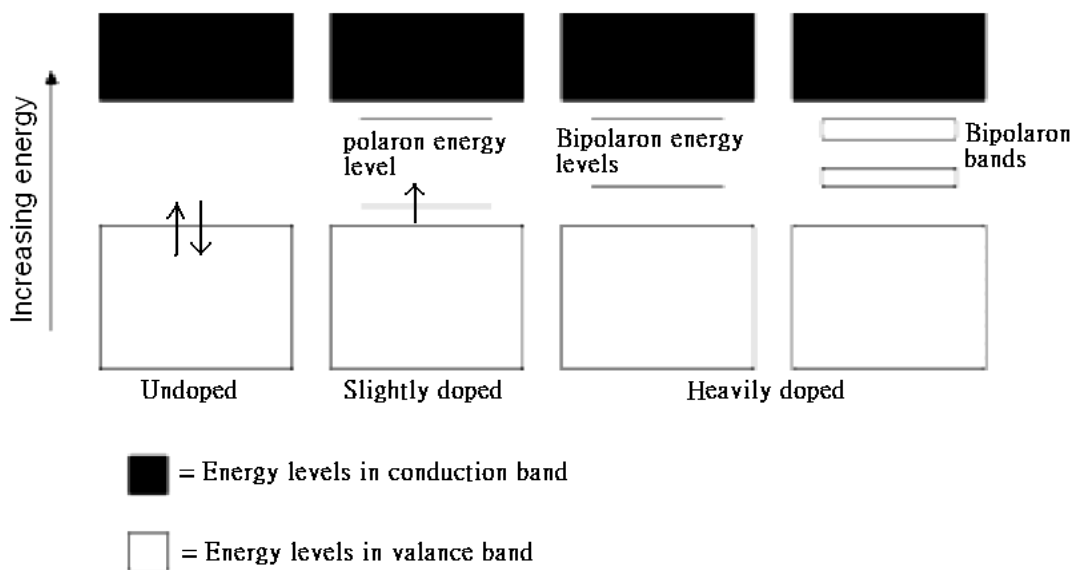


Figure 2.3 The origin of polaron in energy band [8].

2.2.3 Hopping Model

In this theory, scientists introduced that the intermolecular transportation of charge carriers rely on hopping as shown in Figure 2.4. This is a limitation to environment of the charge carrier mobility in organic semiconductor. Hence the phonons could help the hopping of carriers, the mobility decreases with the decreasing temperature. The relation between the mobility of the hopping model and the temperature can be described as the following equation:

$$\mu = \mu_0 \exp[-(T_0 / T)^{1/\alpha}], \text{ where the } \alpha \text{ is ranged from 1 to 4.}$$

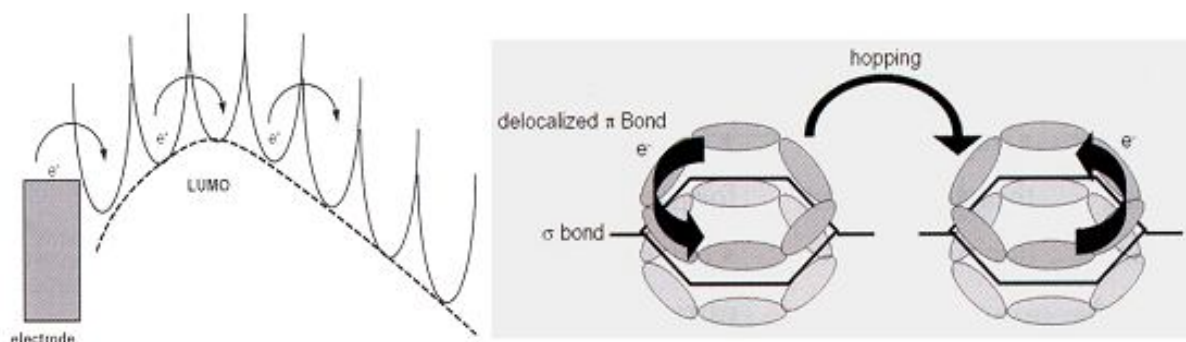


Figure 2.4 Intermolecular charge carrier hopping [55].

2.2.4 Multiple Trapping and Release Model (MTR)

In this model, researchers believed that there existed delocalized levels in the energy gap. These levels are as well as traps of charge carriers, and form a narrow band with high concentration of trap levels. When the charge carriers transport to the delocalized levels, they would be influenced by capture and thermal release. There are two assumptions in MTR model. First, the carriers would be trapped with the probability near 100% in the levels. Second, the release of trap carriers is a process of thermally activated. In this hypothesis, the carriers would contribute to the transportation and the drift mobility is given as following: $\mu_D = \mu_0 \alpha \exp(-E_t / kT)$, where μ_0 is the intrinsic mobility of delocalized levels, α is the ratio between the density of states at the bottom of the band and the concentration of traps, and E_t is the energy level of the defects.

2.3 The Operation of Organic Thin-Film Transistors

2.3.1 Energy Level Principle and Carrier Distribution

The cause of the induced charging from gate bias can be clarified in the simplified energy level diagrams, and it is shown in Figure 2.5. The locations of the HOMO and LUMO of the organic semiconductor relative to the Fermi level of the source and drain contacts at zero gate bias is shown in Figure 2.5a. If a small source and drain bias was applied, there would be no conduction due to no mobile charges in the organic semiconductor. Figure 2.5b and 2.5d show the energy level when applying a positive gate voltage with $V_D = 0$ and $V_D > 0$, respectively. When a positive gate bias is applied, it induces a vertical electric field at the semiconductor/insulator interface. This induced electric field makes the HOMO and LUMO levels in the active layer shift to lower levels. If the gate field is large enough, the LUMO would become resonant with the Fermi levels of the metal contacts, so the electrons can flow

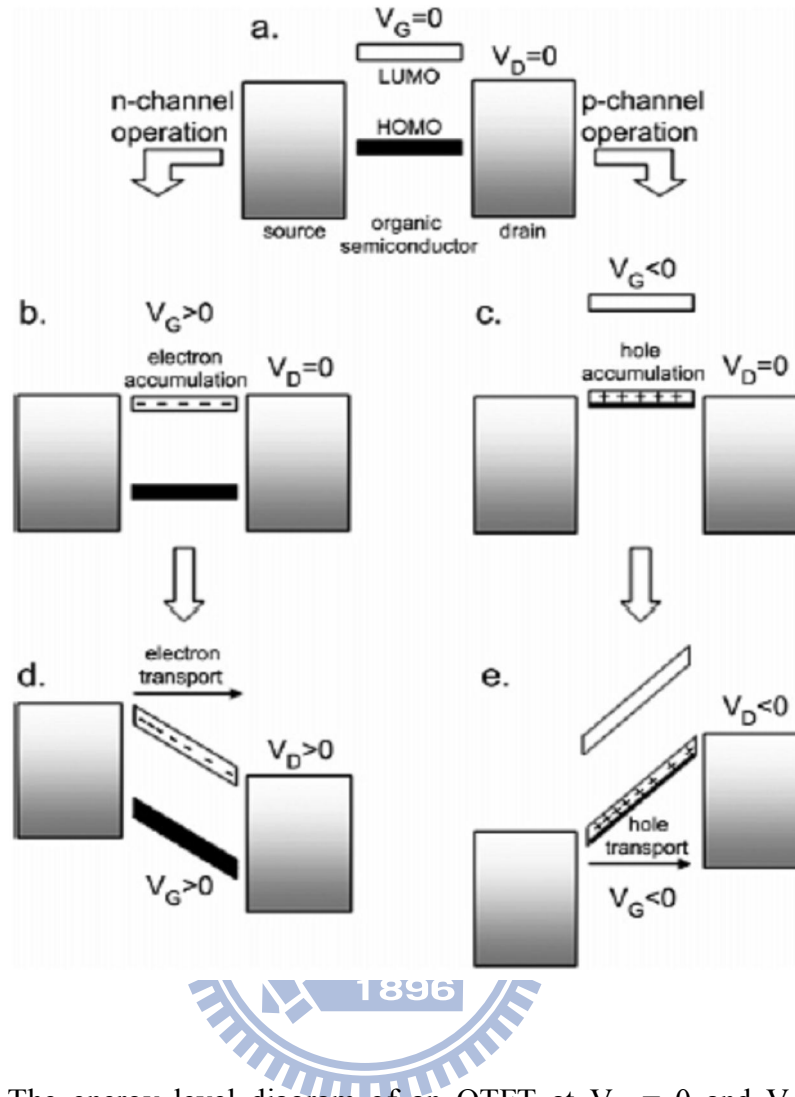


Figure 2.5 (a) The energy level diagram of an OTFT at $V_G = 0$ and $V_D = 0$. (b-e) the mechanism of OTFT operation for the case of electron (b) accumulation and (d) transport; hole (c) accumulation and (e) transport [5].

from the contacts into the LUMO as shown in Figure 2.5b. From the former operation, there are mobile electrons which start to accumulate at the semiconductor/insulator interface then forming a channel between the source and drain electrodes. When applying a drain voltage, it results in electron flow between drain and source as shown in Figure 2.5d. We can explain the situation with negative gate bias by the similar reason as shown in Figure 2.5c and 2.5e. It causes the HOMO and LUMO levels shift to higher levels with applying negative gate bias. The HOMO would become resonant with the Fermi levels of the metal contacts, and then the

holes could accumulate to the semiconductor/insulator interface. In Figure 2.5e, the mobile holes would flow between source and drain as applying a negative drain voltage.

All the former discussions are based on an ideal situation. In fact, the deep traps need to be filled firstly at interfacial states, and then induce extra mobile charges. The additional mobile charge carriers would apply the current in the channel of OTFTs. On the other hand, the V_G have to be biased higher than the threshold voltage (V_T). Therefore we can say that $V_G - V_T$ is the real driving voltage to start to accumulate mobile charge carriers.

Figure 2.6 illustrates the basic operating modes of a TFT. When $V_D \sim 0$, the channel charge density is uniform for a given V_G as shown in Figure 2.6a. The current is nearly linear with V_D in this part. When V_D is nonzero but similar or less than V_G , there is a linear gradient of charge concentration as shown in Figure 2.6b. For a positive V_D , the density of induced charge carriers along the channel (x-direction) is proportional to the voltage difference:

$$q(x) = C(V_G - V_T - V(x)) \quad (\text{C/cm}^2) \quad (2-1)$$

where C (nF/cm^2) is the capacitance of the insulator per unit area. To the terminal of drain, the charge density will be lower, and to the terminal of source, the charge density will be higher. When $V_D = V_G - V_T$, the channel gets pinched-off. There is a depletion part (without free carriers) forming near the drain electrode, and only a space-charge-limited saturation current can flow across this region. If we apply higher V_D , it pushes the pinch point slightly toward source as shown in Figure 2.6c. The channel length in common situation is much longer than the width of this depletion part, the higher V_D would apply no additional drain current.

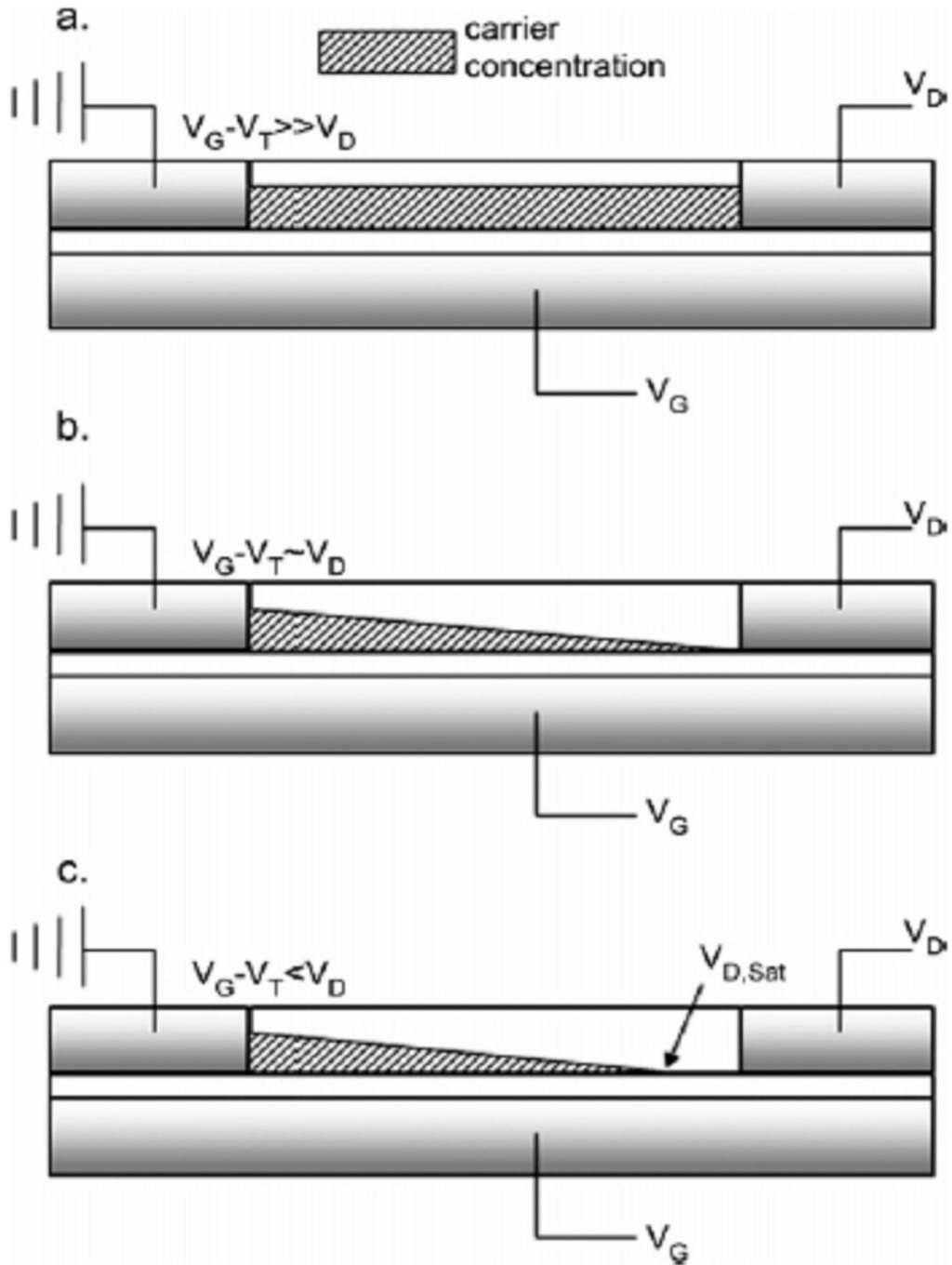


Figure 2.6 (a) Carrier concentration diagram of TFT in the linear regime. (b) Pinch-off occurs when $V_D \sim V_G - V_T$. (c) Carrier concentration diagram of TFT in the saturation regime [5].

2.3.2 The Methods of Extracting Parameters

There are two kinds of electrical characteristic curves. The first plot is I_D - V_D output characteristics by holding V_G constant and sweeping V_D as shown in Fig 2.7a. We can separate this curve into linear and saturation modes. The TFT is operated in linear mode when the V_D is smaller than $V_G - V_T$, and can be considered to be a resistance. When the applying V_D is higher than $V_G - V_T$, the TFT is operated in saturation mode. In this mode, the drain current (I_D) is controlled by V_G .

The second plot is I_D - V_G transfer characteristics by holding V_D constant and sweeping V_G as shown in Fig 2.7b. We can extract many important parameters by this transfer curves such as field-effect mobility, threshold voltage, and on-off ratio. Now we introduce a formula from Ohm's law:

$$\frac{I_D}{tW} = \sigma \frac{V_D}{L} \quad (2-2)$$

where σ is the conductivity, W is the channel width, L is the channel length, and t is the thickness of charged layer in the channel. The equation 2-2 can be rewritten as :

$$I_D = \frac{W}{L} (n_{ind} et) \mu V_D \quad (2-3)$$

where the n_{ind} is the number density of induced charges in the channel, and μ is the carrier mobility. According to equation 2-1, assuming the average value of induced charges is $C(V_G - V_T - V_D/2)$ by a linear gradient in the charge concentration, we obtain:

$$I_D = \frac{W}{L} C \mu [(V_G - V_T) V_D - \frac{1}{2} V_D^2] \quad (2-4)$$

Equation 2-4 is the typical linear regime equation, and it can describe the charge transport in Figure 2.6b.

When $V_D > V_G - V_T$, the TFT is operated in saturation mode and the equation 2-4 will become:

$$I_D = \frac{W}{2L} C \mu_{sat} (V_G - V_T)^2 \quad (2-5)$$

where μ_{sat} is the carrier mobility in saturated regime, and the μ_{sat} is usually higher.

From the above-mentioned discussions, the mobility μ_{sat} can be extracted by differentiating the square root of I_D in saturation mode as:

$$\frac{\partial \sqrt{|I_D|}}{\partial V_G} = \sqrt{\frac{WC}{2L}} \mu \quad (2-6)$$

The slope can be obtained by the $I_D^{0.5} - V_G$ plot in Figure 2.7b. We can also define the V_T by the intersected point of the line on the $I_D^{0.5} - V_G$ plot.

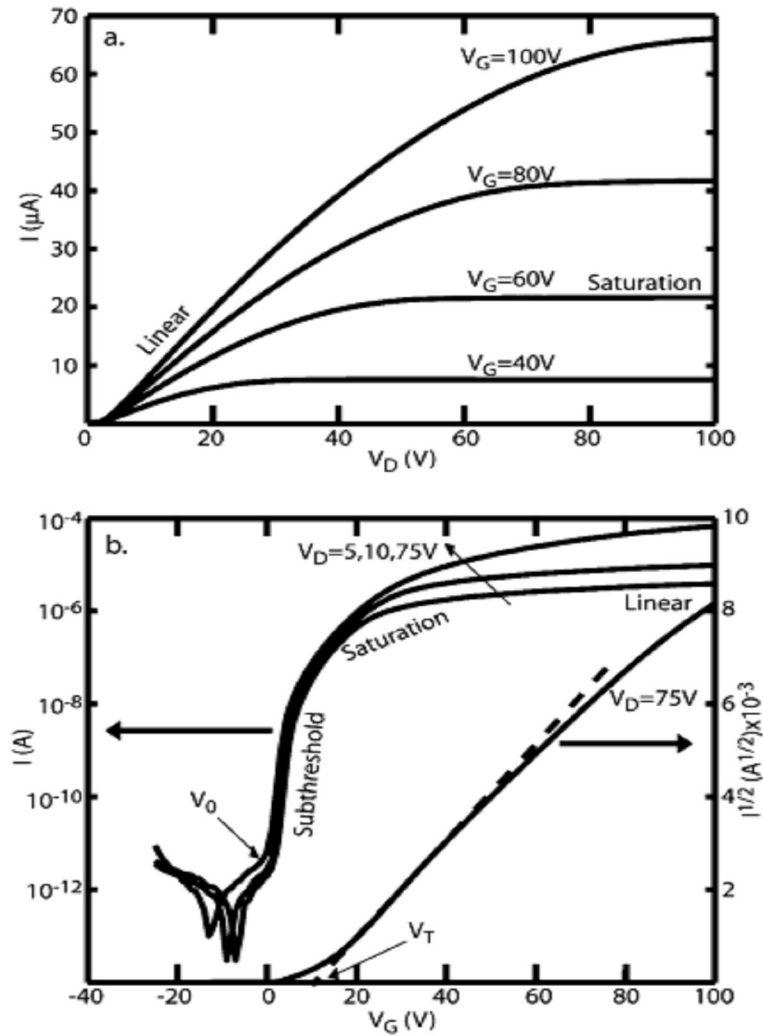


Figure 2.7 (a) $I_D - V_D$ curves for a n-OTFT for various V_G . (b) $I_D - V_G$ curves for various V_D , and the $I_D^{0.5} - V_G$ curve is shown on the right-handed axis [5].

2.3.3 Contact resistance

There are two origins of the TFT series resistance: contact resistance and channel resistance. In recent years, researchers have pointed out that the performances of OTFTs are limited by the contact resistance at metal electrode/organic interface significantly [35-37, 57, 58]. The contact resistance has been found to be comparable with channel resistance. It implies us that the contact resistance plays an important role in determining the electrical characteristics.

We can calculate the contact resistance by the transfer line method:

$$R_{total} = \left(\frac{\partial V_D}{\partial I_D} \right)_{V_D \rightarrow 0}^{V_G = const.} = R_{ch} + R_p = R_{ch} + (R_b + R_c) = \frac{L}{W \mu C (V_G - V_T)} + R_p \quad (2-7)$$

where the R_p is the parasitic resistance, R_c is the contact resistance, R_b is the bulk resistance, and R_{ch} is the channel resistance. We can extract the R_c when the channel length is approaching to zero by equation 2-7 as shown in Figure 2.8 [57].

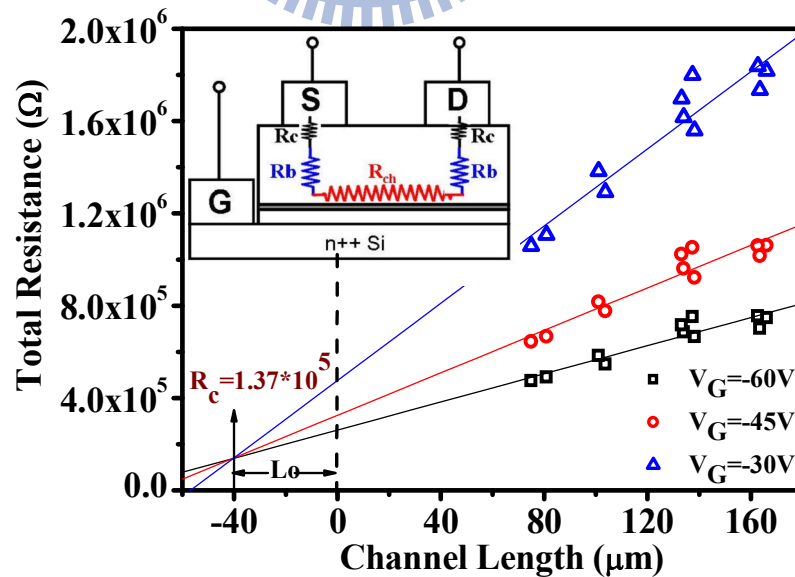


Figure 2.8 The illustration of transfer line method.

Chapter 3

Experimental and Analysis Methods

3.1 Substrate Preparation

3.1.1 Preface

The top-contact structure was chosen to fabricate the n-type OTFTs in this study due to its relatively better performance. The top-contact TFT is shown in Figure 2.1a. ITO (Indium Tin Oxide) is a kind of conducting material which also has high transparency. Because of that, ITO is always coated on glass substrate to form a conducting thin film. In this study, we choose ITO/glass and Si/SiO₂ substrates. With the use of ITO/glass substrate, we usually need to define the ITO pattern by optical lithography. It is attributed to that the polymer insulator often provides a higher leakage current than SiO₂ insulators due to its uniformity and compactness. The cleanness is also an important issue in fabricating OTFT devices. If the substrate is not clean, the uniformity of polymer layer will be low. We will introduce the cleaning process in the following section.

3.1.2 ITO Patterning Process

The process for ITO pattern is shown in Figure 3.1. First, we spin-coated a layer of photoresist (PR) on a cleaned ITO/glass substrate, and then we put shadow a mask that we designed for ITO pattern on the ITO/glass substrate followed by UV exposure for 100 seconds. Second, the exposure parts of PR would become soft and removed in development process. After development, HCl was used to remove the ITO which is with no PR. Finally, the hard PR is removed with acetone.

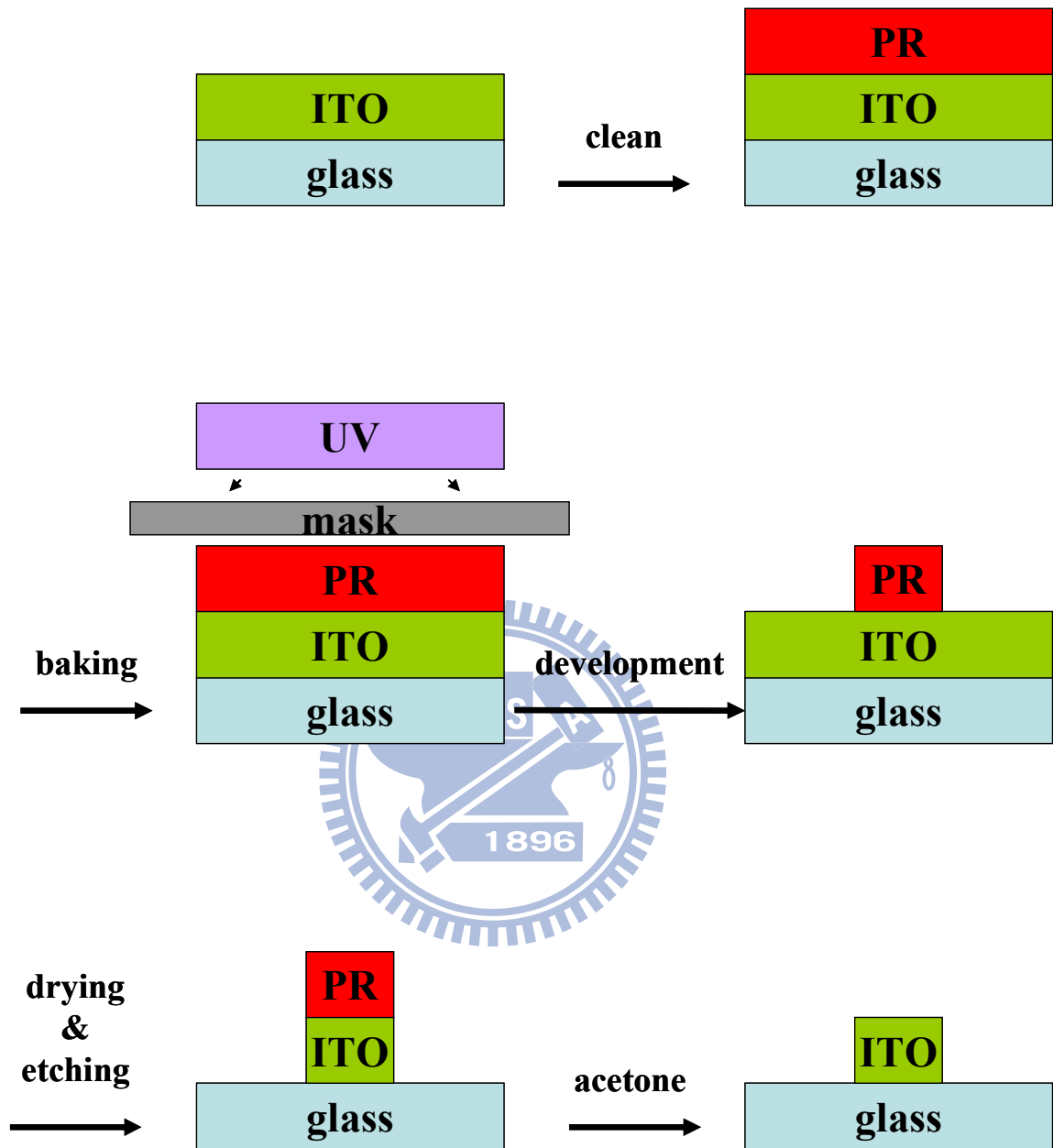


Figure 3.1 The process of ITO patterning.

3.1.3 Cleaning of ITO/Glass Substrate

After etching of ITO, the glass substrates have to be completely cleaned. We washed the substrates with detergent first and rinsed by deionized water in the first place. The detergent can take the large particles and oil sludge away. The second step was soaking the substrates in acetone into an ultrasonic cleaner for 40 minutes. Organic pollutants would be swept away in this step. After rinsing by DI water in 5 minutes, we put the substrate in isopropyl alcohol (IPA) with ultrasonic microvibrations for 30 minutes. The residual acetone and water molecules would be taken away by IPA. Finally, we dried the substrates by nitrogen shower, and then these substrates are placed into an oven in which the temperature was set to 120°C for at least 24 hours to remove the water.

3.1.4 Cleaning of SiO₂/Si Substrate

We also use heavily doped n-type silicon wafers, with thermal SiO₂ to fabricate the devices. The top SiO₂ layer was 200 nm-thick, and the sheet resistance was about 0.001~0.003 ohm-cm. The capacitance per unit area in the SiO₂ layer was 14.2 nF/cm².

First, we put the substrates into a Teflon container, and rinsed them with DI water for 5 minutes. Then we dipped the container into a 3:1 mixture of concentrated sulfuric acid (H₂SO₄) and hydrogen peroxide (H₂O₂) at 80°C for 20 minutes. After this acid bath, we rinsed the substrates with DI water again for 5 minutes. Finally, we dried the substrates with nitrogen flow, and put them into a hot oven to remove the residual water.

3.2 The Materials

[6,6]-phenyl C₆₁-butyric acid methyl ester (PCBM) [Figure 3.2(a)] was used as the active layer of the TFTs. We dissolved PCBM molecules in chloroform (CF) [Figure 3.2(b)]. The polymer poly(ethylene glycol) (PEG) [Figure 3.2(c)] has blended into the PCBM layer. The dielectric polymer film was made of poly(4-vinylphenol) (PVP) [Figure 3.2(d)] and poly(melamine-co-formaldehyde) methylated (PMCFM) [Figure 3.2(e)]; they were dissolved in propylene glycol monomethyl ether acetate (PGMEA) [Figure 3.2(f)].

The energy level diagram of the materials used in this study is displayed in Figure 3.3.

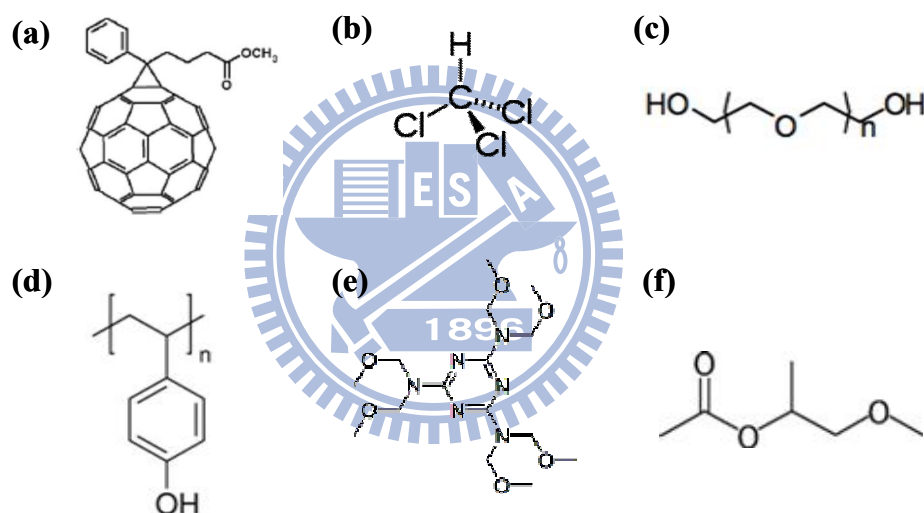


Figure 3.2 The structure of organic materials used in this experiments.

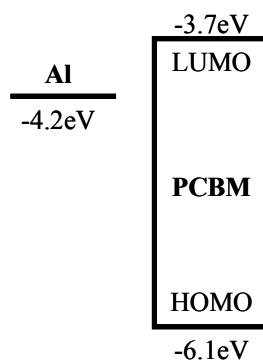


Figure 3.3 The energy level diagram of the materials used in this study.

3.3 Device Fabrication Process of OTFTs

3.3.1 Spin-Coating Polymer Dielectric Film

The OTFT was fabricated on a ITO/glass substrate ($<10 \text{ } \Omega/\text{sq}$ sheet resistance), where ITO was used as gate electrode. Before spin-casting of the polymer insulator, we put the substrates into an UV-Ozone machine for 30 minutes. The ozone molecules would burn the organic contaminant on substrates, and then be taken away by cleaning air flow.

The cleaned ITO substrates were then covered with a layer of 760-nm-thick polymer dielectric insulator, which was prepared by spin-coating of a solution of PVP (11wt%) and PMCFM (4wt%) (cross-linking agent) in PGMEA. The other OTFT was prepared on SiO_2 substrate then covered with a layer of 50-nm-thick PVP interlayer.

The PVP films were firstly baked at 120°C for 5 minutes and then 200°C for 30 minutes. The resulting capacitances per unit area of the insulator on ITO and the interlayer on SiO_2 were 5.4 and $10.0 \text{ nF}/\text{cm}^2$, respectively.

3.3.2 Spin-Coating of PCBM/PEG Blends as the Active Layer and Evaporation of Metal Electrodes

The PCBM/PEG blended film was spin-coated on the PVP coated substrate inside a N_2 -filled glove box. The spin rate was set to 1000 r.p.m. for 30 seconds.

Before the deposition of S/D, the device was pre-annealed at 80°C for 15 min. Finally, Al was thermally evaporated onto the active layer under a pressure less than 5×10^{-6} torr through a shadow mask to form S/D contacts. The thickness of Al S/D was 100 nm. The channel length and width were 100nm and $2000 \mu\text{m}$, respectively.

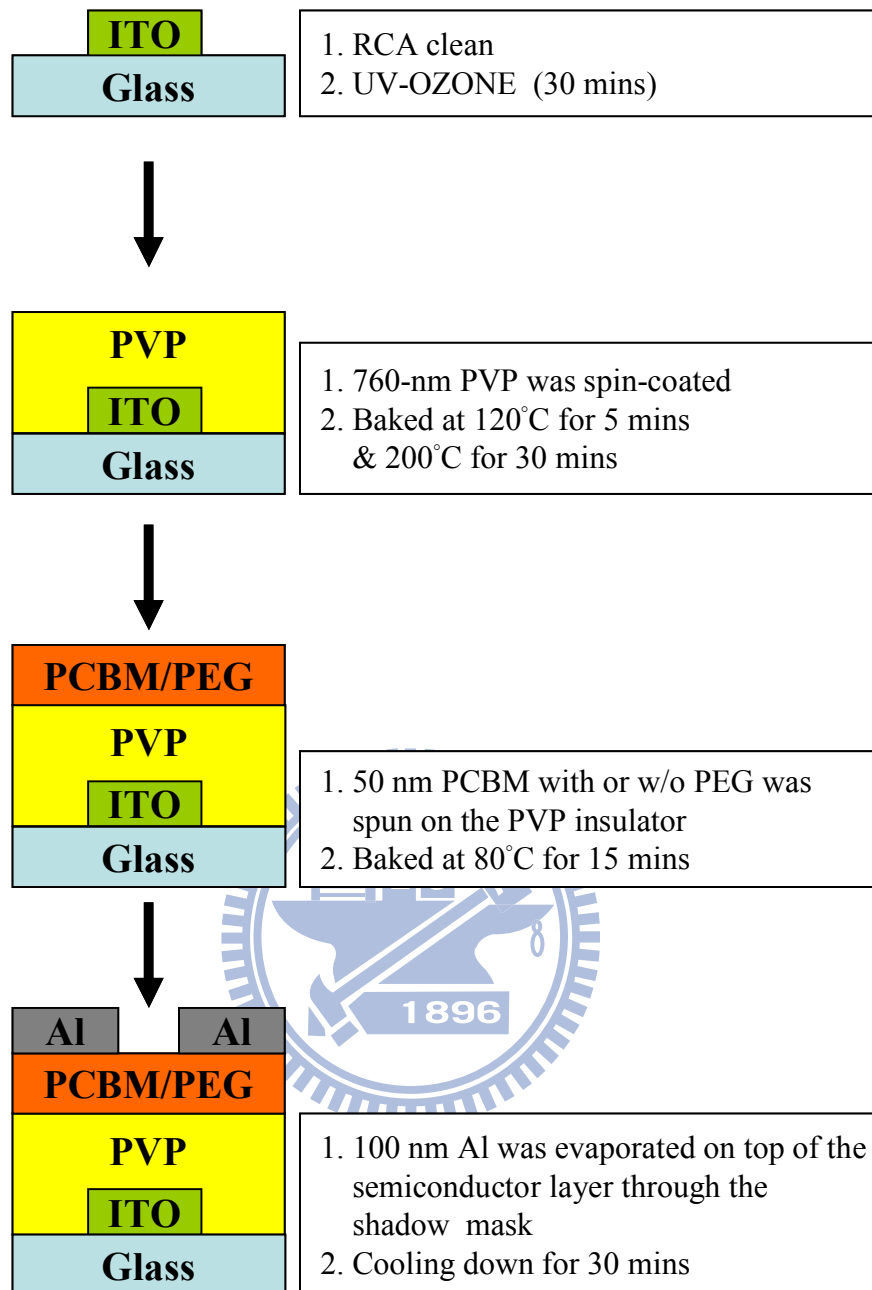


Figure 3.4 The flow chart of the device fabrication process (ITO/glass substrates).

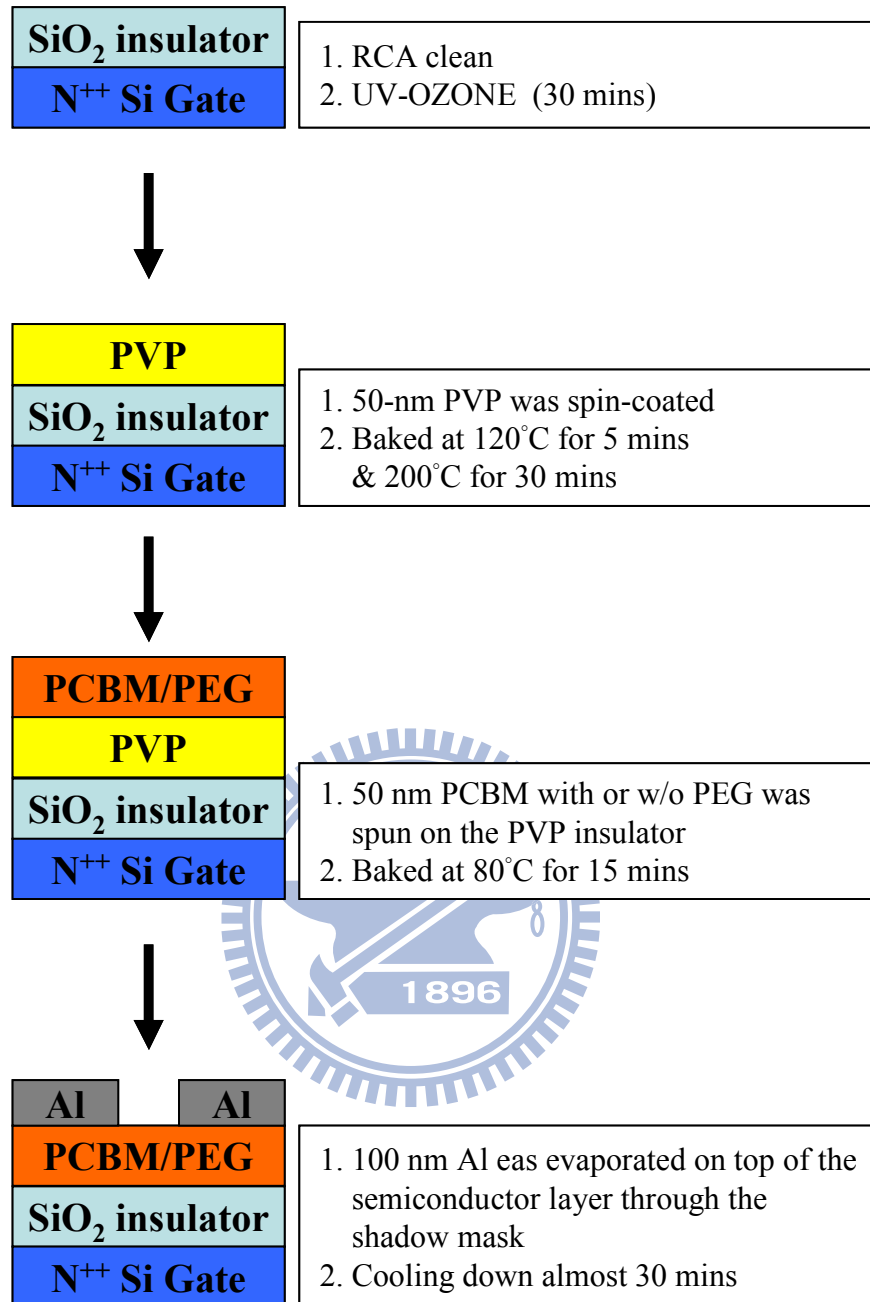


Figure 3.5 The flow chart of the device fabrication process (Si/SiO₂ substrates).

3.4 Measurements and Analysis of OTFTs

3.4.1 Electrical Characteristics

In this work, we measured the electrical properties of the devices by Keithley 4200 IV measurement system at room temperature. For PCBM devices, we apply a positive gate voltage to accumulate electrons in the channel near the semiconductor/insulator interface. In the I_D - V_D measurement, we swept the gate bias from 0 to 60V, and the gate voltage step was 15 V from $V_G = 0$ V to $V_G = 60$ V. Additionally, in the I_D - V_G measurement, we swept the drain voltage from -20 V to 60 V, and the drain voltage step was from 15V to 60V.

3.4.2 Capacitance Analysis

We measured the capacitances of SiO_2 and PVP cross-linked polymer by HP 4284A using metal-insulator-metal (MIM) structure.

3.4.3 Surface Morphology Measurement

The atomic force microscope (AFM) has been invented in 1985, which could measure the surface morphology of low conductivity materials. The principle of AFM is the interaction of van der Waals force, which is different with scanning electron microscope (SEM) by electron tunneling effect. We assume there are two atoms: one is on the tip of the cantilever, the other is on the surface of sample. The interaction force between the two atoms depends on their distance as show in Figure 3.6. In this study, we used Digital Instruments Dimension 3100 AFM to get the surface morphology of the active layer. Figure 3.7 shows how can AFM work to obtain surface properties.

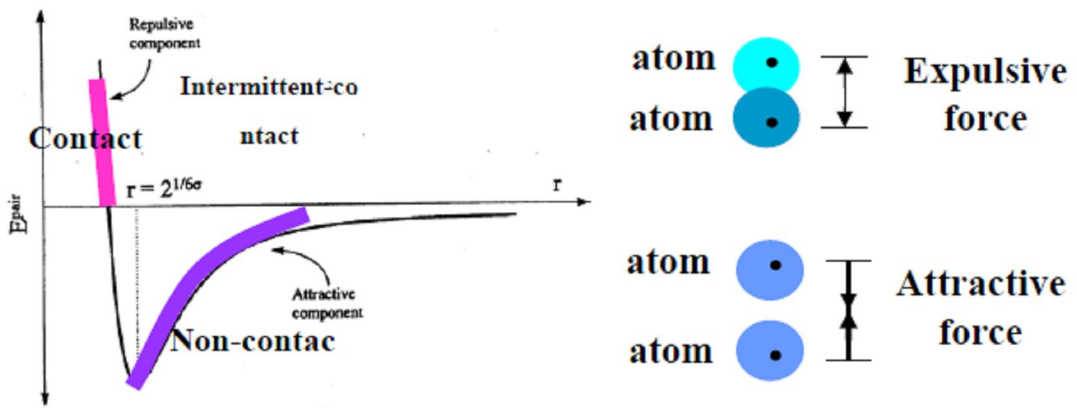


Figure 3.6 The interaction force between two atoms.

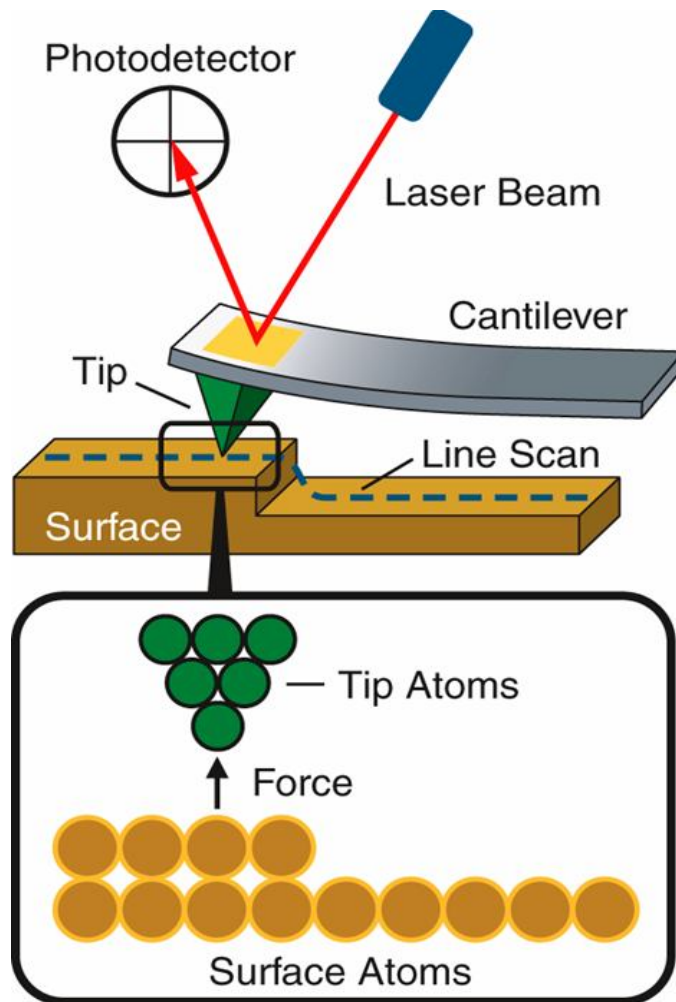


Figure 3. 7 The operation method of AFM.

3.4.4 X-ray Photoelectron Spectroscopy Measurement

X-ray photoelectron spectroscopy (XPS) is a quantitative spectroscopic technique that measures the elemental composition, chemical state and electron state of the elements that exist in materials. The basic components of XPS system is shown in Figure 3.8. XPS spectra are obtained by irradiating a material with a beam of X-rays while measuring the kinetic energy and number of electrons that escape from the top thin-film (1 to 10 nm) of the material being analyzed simultaneously. XPS requires ultra high vacuum (UHV) conditions. XPS detects all elements with an atomic number (Z) of 3 (lithium) and above. It cannot detect hydrogen ($Z = 1$) or helium ($Z = 2$). XPS is routinely used to analyze inorganic compounds, metal alloys, semiconductors, polymers, catalysts, glasses, make-up, teeth, bones, and many others.

From XPS measurement, we can know if there is any chemical interaction between PEG and Al S/D electrodes. In 2006, Guo *et al.* reported that the performances of polymer light-emitting diodes could be improved by the formation of a PEGDE (PEG dimethyl ether)/Al complex at the cathode interface [58]. In Figure 3.9, the C1s XPS spectrum of the HY-PPV/Al has a main peak at a binding energy 284.6 eV. The peak is associated with hydrocarbon atoms. When an additional PEGDE modify layer (2.5 nm) was inserted on the surface of the HY-PPV layer with Al, the C1s peak at 288.6 eV grew. PEGDE is a polymer with the same sequent carbon-oxide functional group like PEG, $(-\text{CH}_2\text{CH}_2\text{O}-)_n$, so a chemical reaction between the lone-pair electrons and Al in the oxygen atoms of the PEGDE chains was expected. The C1s diagram at 288.6 eV is related to the formation of the organic oxide/Al complex. Due the former results, we expect that PEG would react with Al and we can get the information from the XPS measurement.

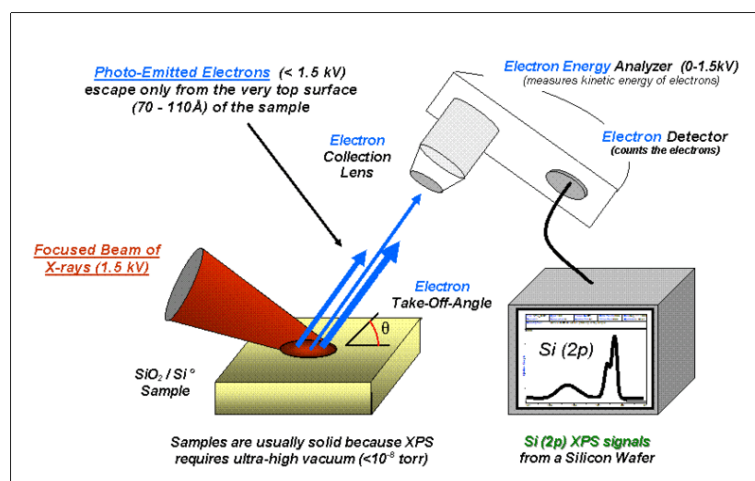


Figure 3.8 Basic components of monochromatic XPS system.

[Adapted from http://en.wikipedia.org/wiki/X-ray_photoelectron_spectroscopy]

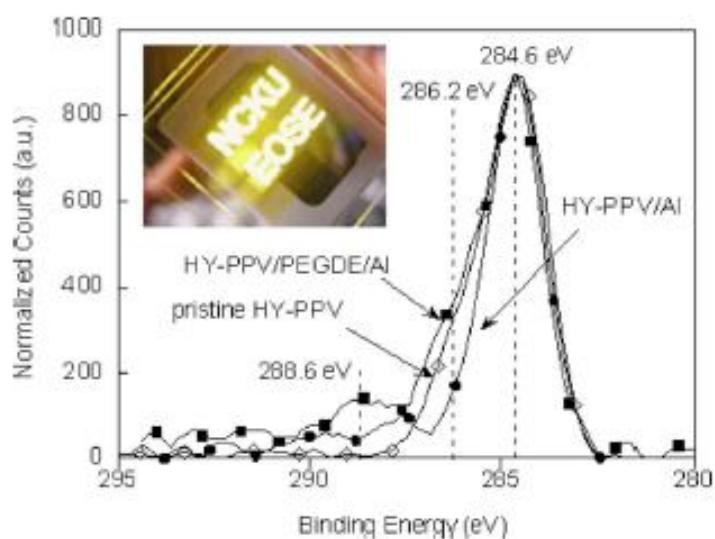


Figure 3.9 XPS C1s spectra of pristine HY-PPV (\diamond), HY-PPV / Al (\bullet), and HY-PPV / PEGDE / Al [58].

Chapter 4

Results and Discussion

4.1 Characteristics of Device Electrical Properties

4.1.1 The Effect of Molecular Weight of PEG

We measured these devices prepared with various molecular weight of PEG in a N₂-filled glove box, where the concentrations of O₂ and H₂O were less than 1 ppm. Figure 4.1 illustrates the I_D-V_D electrical properties of these devices. Figure 4.1(a) shows the characteristic of pristine 1wt% PCBM device. From 4.1(b)-(f) represent the devices prepared whose molecular weight (M.W.) was with PEG 400, 1000, 3000, 8000, and 20000, respectively. All the weight ratio of PEG:PCBM is 1:20. The device with pristine PCBM has the lowest drain current in the saturation regime, and the device prepared with PEG 20000, meaning the M.W. was 20000 had a three-times higher drain current than that of pristine PCBM TFT. We can find that when the larger molecular weight of PEG blending, we could get higher drain current.

The I_D-V_G characteristics are shown as Figure 4.2. The data shown in Figure 4.2 were measured at V_D = 60V and V_G was swept from -20 to 60 V. Furthermore, the electron mobility was calculated from slopes of square root of drain current versus gate voltage in the saturation regime [Figure 4.2(b)]; the important electrical characteristic parameters were summarized in Table 4.1. The device prepared with PEG 20000 had higher on-off current ratio (4.1×10^4), and exhibited a showed lower threshold voltage (-2.61V). The mobility (0.0440 cm²/Vs) also became three times larger then that of pristine device (0.0141 cm²/Vs). The value of electron mobility is comparable with that of the device made with a Cs₂CO₃ buffer layer on Al electrodes (0.0445 cm²/Vs) [37].

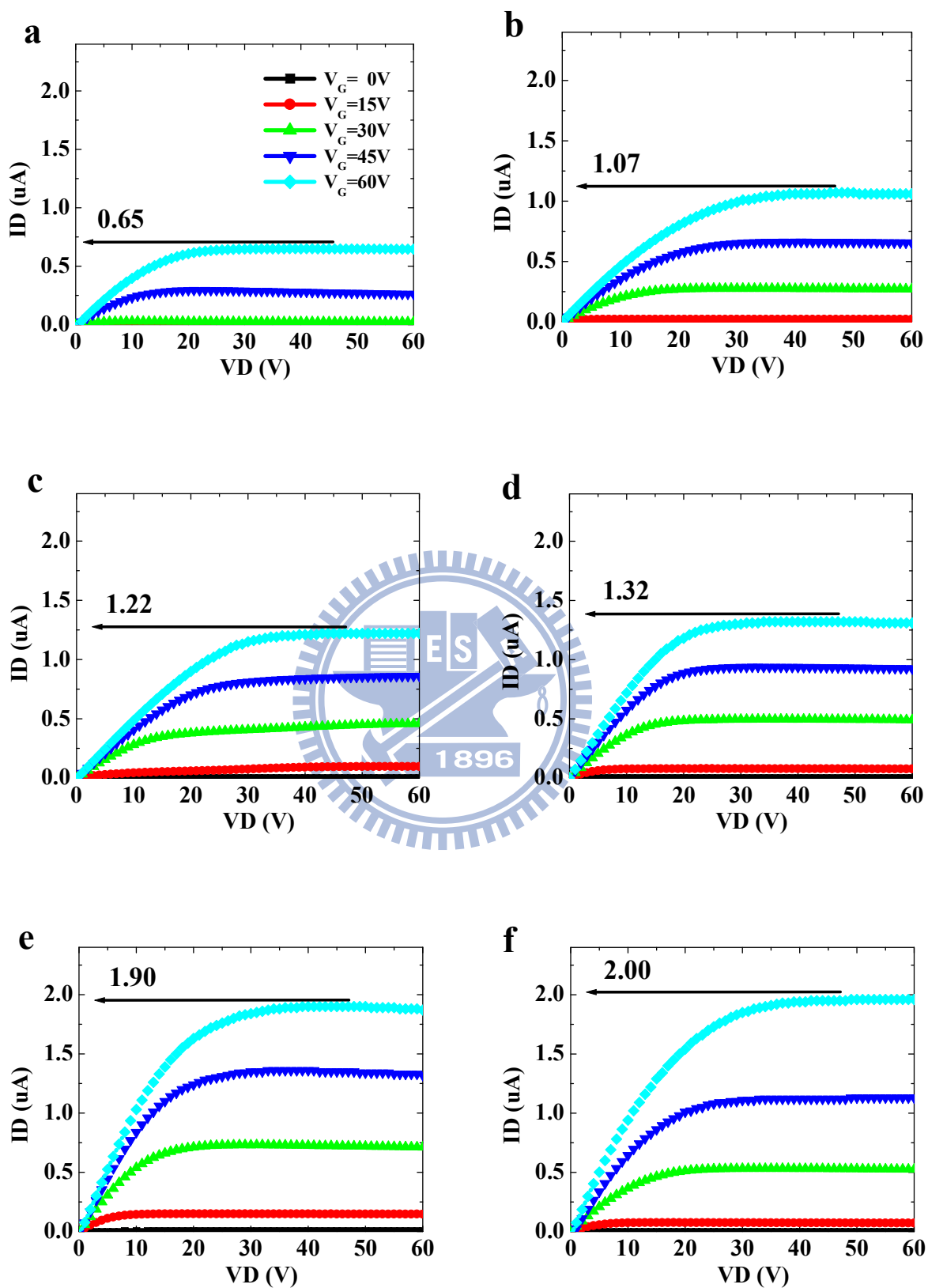


Figure 4.1 The I_D - V_D output curves of (a) pure PCBM device, and device prepared with PEG (b) 400, (c) 1000, (d) 3000, (e) 8000, and (f) 20000, respectively.

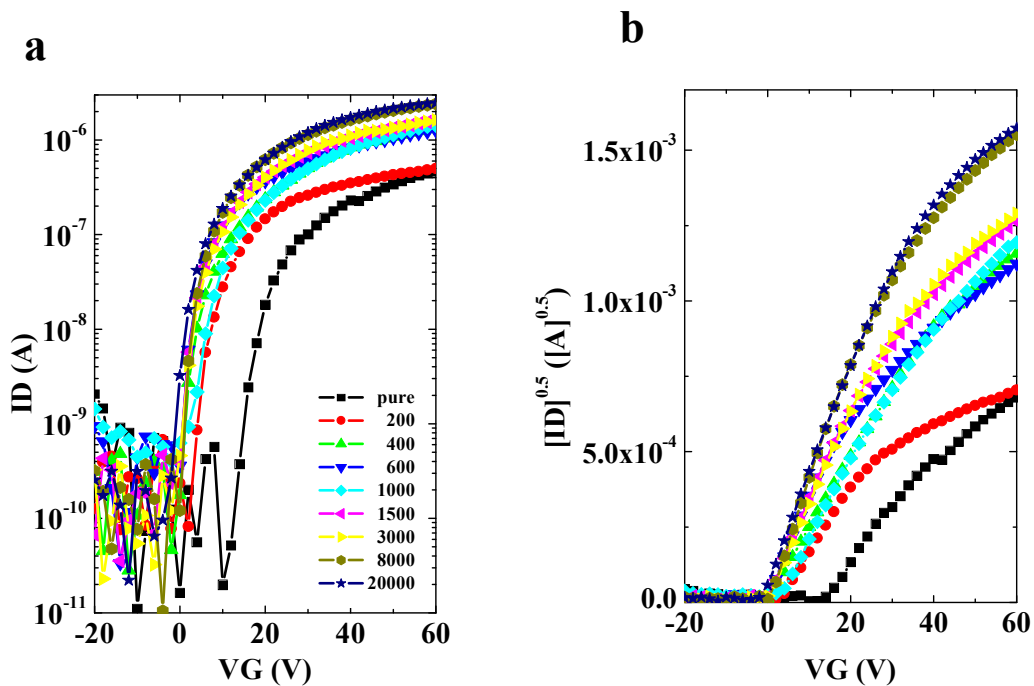


Figure 4.2 The (a) I_D - V_G and (b) $I_D^{1/2}$ - V_G transfer curves at $V_D = 60V$ with distinct molecular weight of PEG blending.

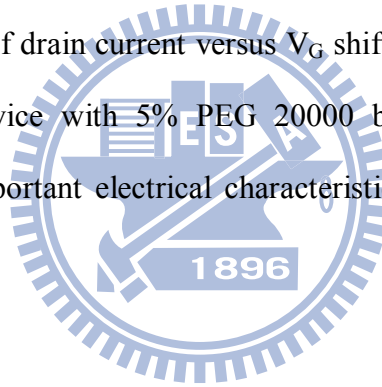
Table 4.1 The parameters of the OTFTs with distinct PEG molecular weight (MW) blending measured in nitrogen filled glove box.

MW of PEG (g/mol)	Mobility (cm^2/Vs)	V_T (V)	On-off ratio
Pure PCBM	0.0141	17.02	0.6×10^4
200	0.0145	4.78	1.2×10^4
400	0.0215	0.84	1.4×10^4
600	0.0245	-0.56	1.1×10^4
1000	0.0264	-0.74	1.2×10^4
3000	0.0285	-0.20	1.1×10^4
8000	0.0376	-0.90	2.0×10^4
20000	0.0440	-2.61	4.1×10^4

4.1.2 The Effect of PEG Concentration

In this section, the effect of PEG concentration is investigated. Figure 4.3 illustrates the I_D - V_D electrical performances of different devices. Figure 4.3(a) shows the characteristic of pure-PCBM device. Figure 4.3(b) to 4.3(f) represent the output curves of the devices prepared with 1%, 5%, 8%, 11% and 16% PEG (M.W.=20000), respectively. From the figures, we can find that the saturation drain current increased with increasing PEG concentration. However, while the weight ratio of PEG excess 5 wt%, the value of saturation drain current became lower as shown from Figure 4.3(d) to 4.3(f).

The I_D - V_G transfer characteristics are shown in Figure 4.4. All the devices were measured at $V_D = 60$ V and V_G bias was swept from -20 V to 60 V. The threshold voltage extracted from square root of drain current versus V_G shifts negatively due to the higher ratio of PEG blending. The device with 5% PEG 20000 blending shows the best electrical performance. The other important electrical characteristic parameters were shown in Table 4.2.



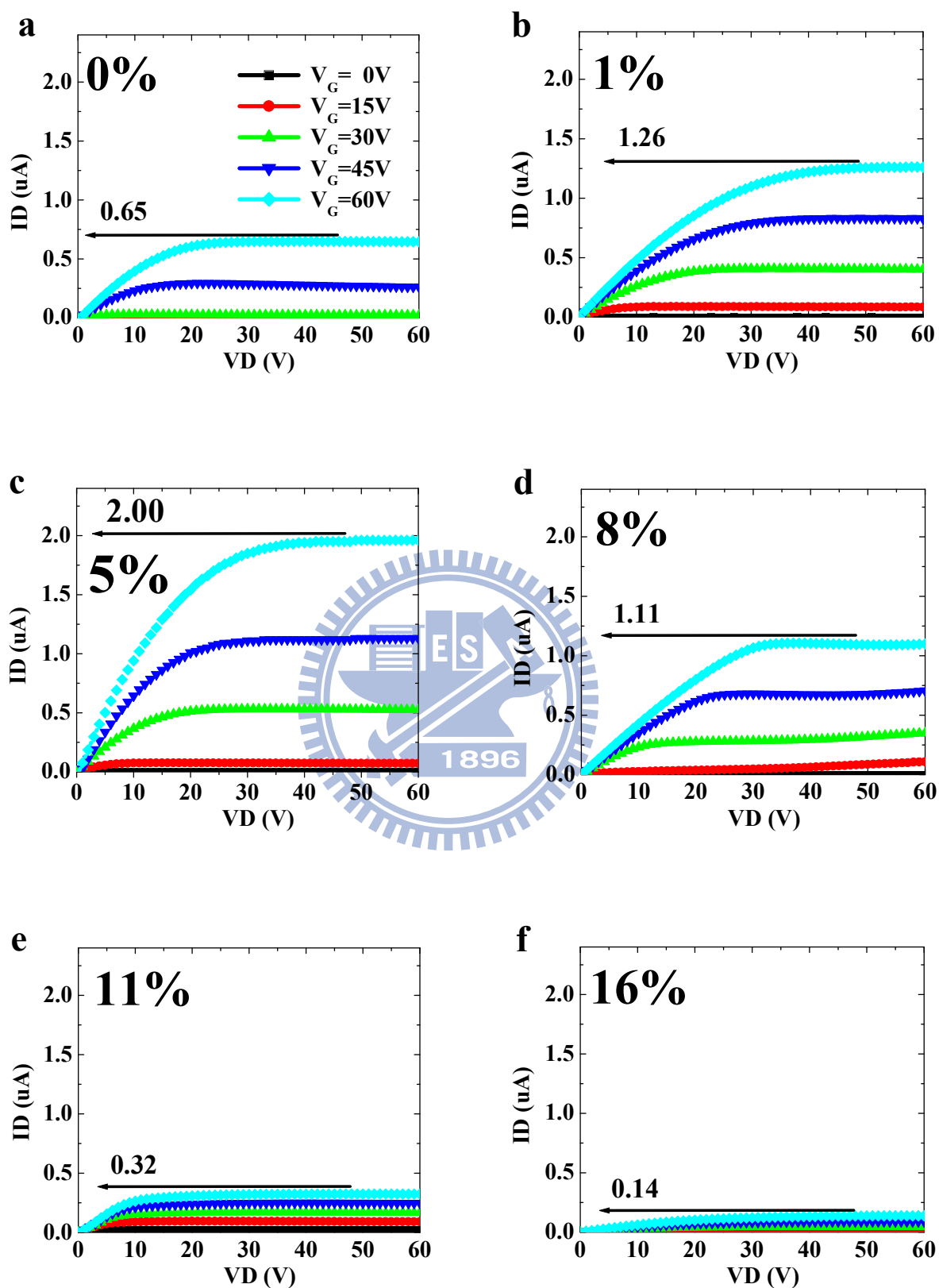


Figure 4.3 The I_D - V_D output curves of (a) pure PCBM OTFTs, and with (b) 1%, (c) 5%, (d) 8%, (e) 11%, and (f) 16% PEG 20000 blending, respectively.

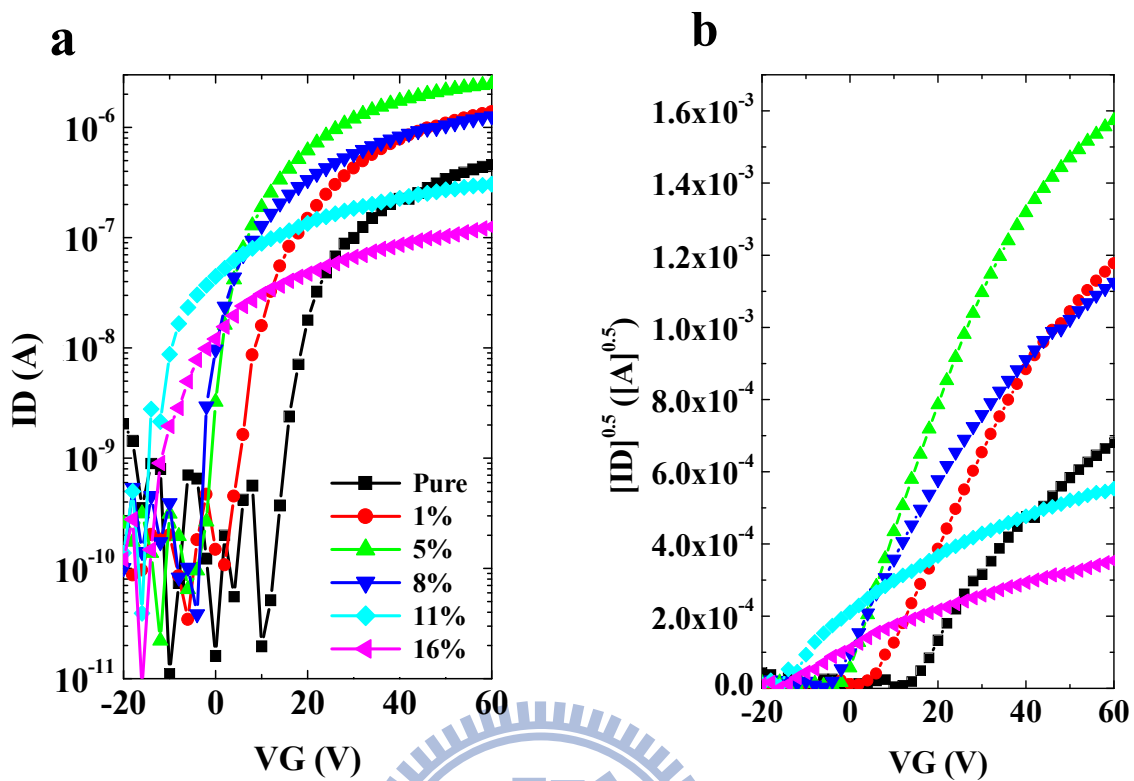


Figure 4.4 The (a) I_D - V_G and (b) $|I_D|^{1/2}$ - V_G transfer curves at $V_D = 60V$ with distinct concentration of PEG 20000 blending.

Table 4.2 The parameters of the OTFTs with different ratio PEG 20000 blending measured in nitrogen filled glove box.

Weight ratio of PEG (wt%)	Mobility (cm^2/Vs)	V_T (V)	On-off ratio
Pure PCBM	0.0141	17.02	0.6×10^4
1	0.0241	6.13	1.3×10^4
5	0.0440	-2.61	4.1×10^4
8	0.0211	-3.54	1.2×10^4
11	0.0098	-14.19	0.8×10^4
16	0.0014	-14.21	1.5×10^4

4.1.3 The Electrical Characteristics Measured in the Atmosphere

We try to measure these devices in ambient environment in which the relative humidity was about 60%. Figure 4.5 illustrate the I_D - V_D electrical output performances prepared without [Figure 4.5(a)] and with [Figure 4.5(b)] PEG 1500. The device with PEG1500 (5%) blending had much higher saturation drain current.

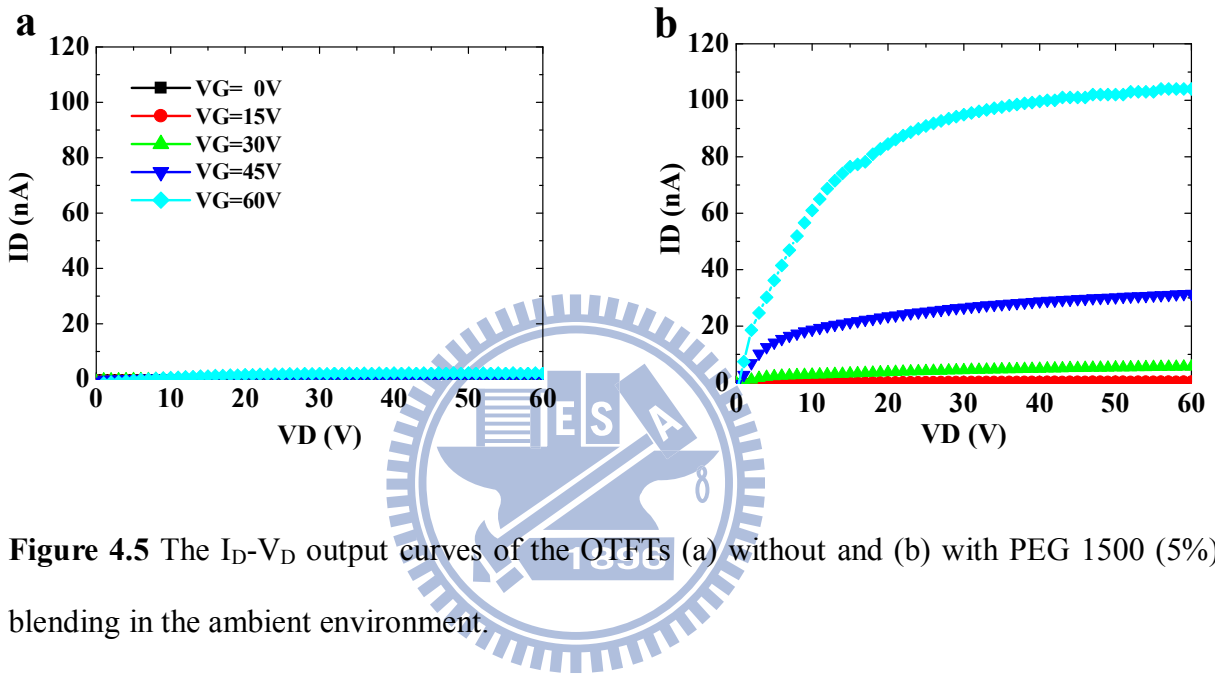


Figure 4.5 The I_D - V_D output curves of the OTFTs (a) without and (b) with PEG 1500 (5%) blending in the ambient environment.

Table 4.3 The comparison of transfer characteristics of the OTFTs measured in inert and ambient environment.

	Mobility (cm^2/Vs)	V_T (V)	On-off ratio
Pure (inert)	1.41×10^{-2}	17.02	0.6×10^4
Pure (ambient)	3.19×10^{-5}	23.35	0.05×10^4
PEG (inert)	2.64×10^{-2}	-0.74	1.2×10^4
PEG (ambient)	2.04×10^{-3}	18.58	0.2×10^4

Figure 4.6 shows the I_D - V_G transfer output performance and it suggests that the pure-PCBM OTFT showed a poor and unstable electrical characteristic in the ambient environment. On the other hand, the device with PEG shows a relatively higher drain current although it was still prepared lower than that of the device measured in an inert environment. Table 4.3 summarizes the transfer performances of these devices in the ambient atmosphere. For the device prepared without PEG, the threshold voltage shifted from 17.02 to 23.35 V and the mobility decreased from 1.4×10^{-2} to 3.2×10^{-5} cm^2/Vs . After the addition of PEG, the threshold voltage shifted from -0.74 to 18.58 V and the mobility decreased from 2.6×10^{-2} to 2.0×10^{-3} cm^2/Vs . The mobility of the pristine PCBM device encountered three order decay; but the mobility of PEG 1500 device decayed by just one order of magnitude. Even though the performance measured in the ambient environment was still decayed, PEG blending in active layer might be a good method to protect the channel.

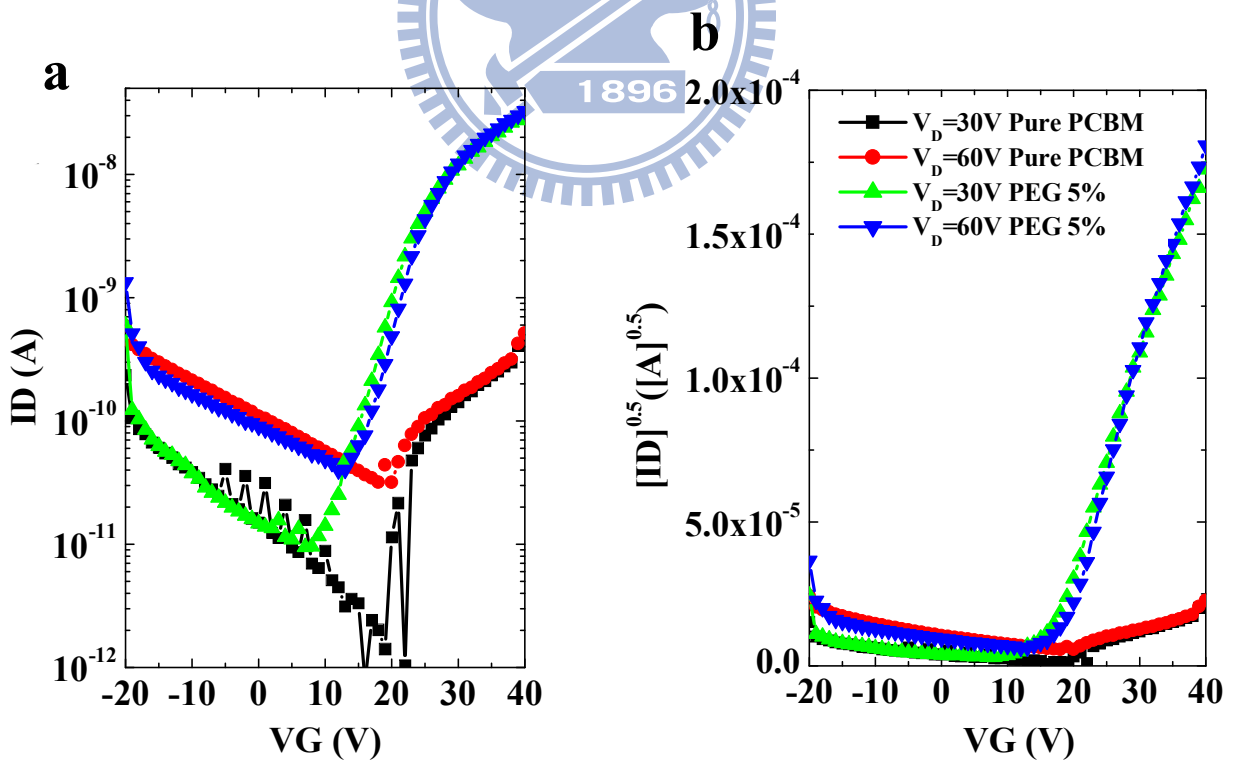


Figure 4.6 The (a) I_D - V_G and (b) $I_D^{1/2}$ - V_G transfer curves at $V_D = 30$ V and 60 V of the OTFTs with and without PEG blending in ambient environment.

4.1.4 The Effect of PEG on the Devices Fabricated on PVP/SiO₂

Substrate

We measured the devices prepared with PCBM/PEG 400 composition fabricated on PVP/SiO₂ substrates. Figure 4.7 illustrates the I_D - V_D electrical performances measured in inert environment. The device with pristine-PCBM has lower drain current in the saturation regime. The device with PEG blending has two times higher drain current than that of pristine-PCBM OTFT. The data shown in Figure 4.8 were measured at $V_D = 60$ V, and V_G bias swept from -20 to 60 V. The device prepared with PEG 400 had higher on-off current ratio (9.0×10^3), and then showed large threshold voltage shift (from 31 V to 5 V). The other important extracted parameters were summarized in Table 4.4.

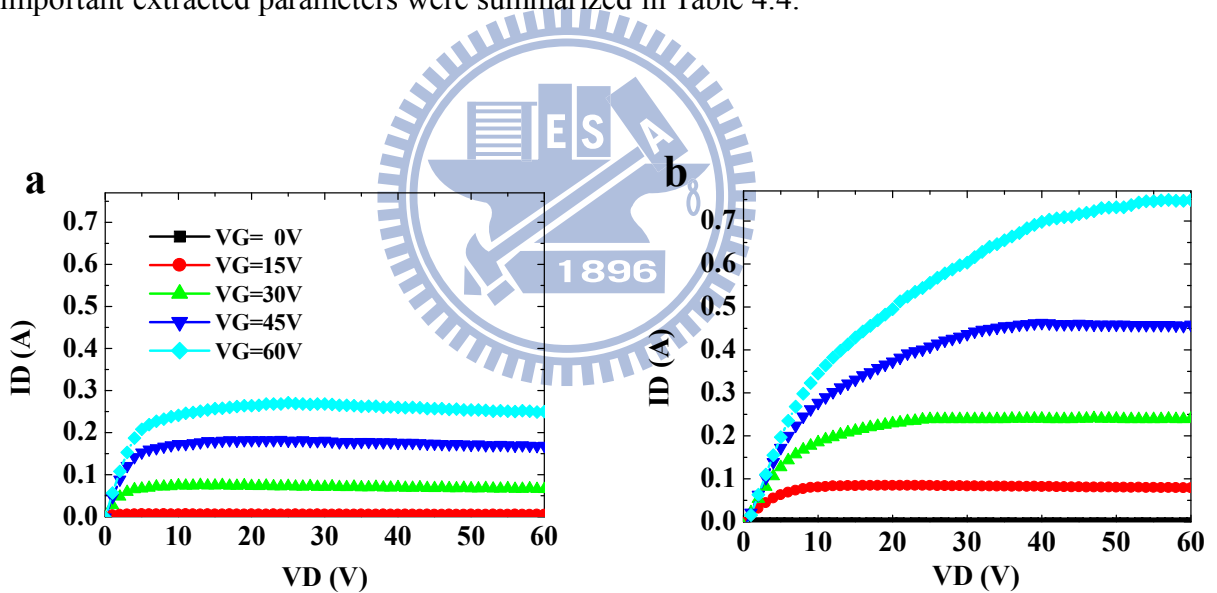


Figure 4.7 The I_D - V_D output curves of the OTFTs prepared (a) without, and (b) with PEG 400 on PVP/SiO₂ substrates.

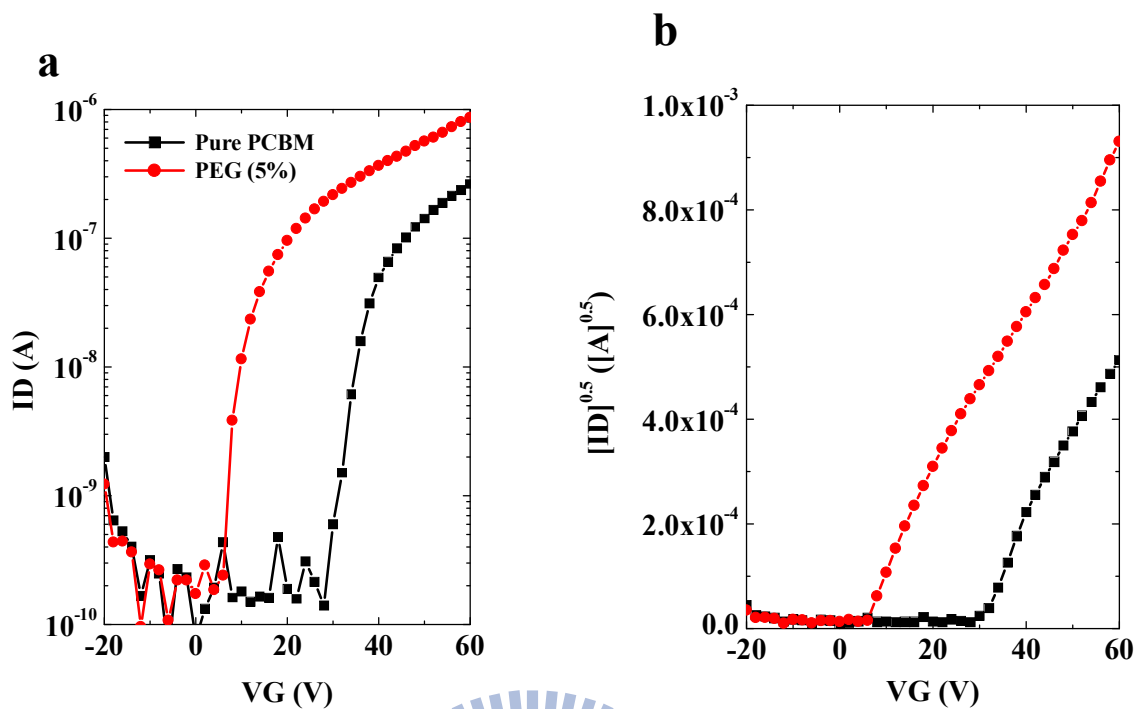


Figure 4.8 The (a) I_D - V_G and (b) $I_D^{1/2}$ - V_G transfer curves at $V_D = 60$ V of the OTFTs with and without PEG blending on PVP/SiO₂ substrates.

Table 4.4 The parameters of the OTFTs prepared with and without PEG blending on PVP/SiO₂ substrates.

PVP/SiO ₂ substrate	Mobility (cm ² /Vs)	V_T (V)	On-off ratio
Pure	0.0059	31.08	3.4×10^3
PEG (5%)	0.0060	5.32	9.0×10^3

We further measured these devices seven times after first test. Interestingly, the electrical performances of pure PCBM OTFT decayed strongly and fast. After the addition of PEG 400, the device became more robust. The V_{ON} shifts of the devices with and without PEG blend were 16 and 8 Volts, respectively, and the loss of saturation drain current at $V_{DS} = 60$ V with and without PEG blended were 19 and 69 %, respectively. PEG molecular perhaps play a role

to improve the stability. The detailed data are shown in Table 4.5 (pure PCBM) and 4.6 (PEG blended).

Table 4.5 The continuous measurement parameters of the pristine PCBM OTFT on PVP/SiO₂ substrates in N₂-filled glove box.

Measurement (times)	Mobility (cm ² /Vs)	V _T (V)	V _{ON} (V)	I _{sat.} (A)	On-off ratio
1 st	0.0038	28.49	26	0.26×10 ⁻⁶	1.6×10 ³
3 rd	0.0045	35.40	34	0.20×10 ⁻⁶	1.0×10 ³
5 th	0.0057	40.24	40	0.17×10 ⁻⁶	1.0×10 ³
7 th	0.0026	40.50	42	0.08×10 ⁻⁶	0.8×10 ³

Table 4.6 The continuous measurement parameters of the PEG (5%) /PCBM OTFT on PVP/SiO₂ substrates in N₂-filled glove box.

Measurement (times)	Mobility (cm ² /Vs)	V _T (V)	V _{ON} (V)	I _{sat.} (A)	On-off ratio
1 st	0.0079	10.73	10	0.67×10 ⁻⁶	3.4×10 ³
3 rd	0.0079	12.58	14	0.64×10 ⁻⁶	4.8×10 ³
5 th	0.0094	16.66	16	0.58×10 ⁻⁶	3.8×10 ³
7 th	0.0101	18.87	18	0.54×10 ⁻⁶	3.3×10 ³

4.2 Morphological Analysis of the Active Films

The height-mode images of the PCBM films prepared with different molecular weight of PEG were displayed in Figure 4.9. Figure 4.9(a) showed the image of pristine-PCBM film deposit on a PVP film. Figure 4.9(b)-(f) represent the images of the films prepared with PEG 400, 1000, 3000, 8000, and 20000, respectively. All the blending ratio of PEG:PCBM was 1:20. The data scale is 7 nm. The film containing no PEG exhibits a smooth surface morphology. After blending 5% PEG into the film, "holes-like" images was present on the surface of the film. When increasing the PEG molecular weight, much more holes emerged. The 5% PEG 20000 blending sample covered a biggest area. Because the concentration of the PEG is 5%, we would not expect the PEG phase to cover the whole surface. Therefore, we suspect that the distribution of PEG molecules was uneven and that phase separation in a direction normal to the substrate occurred in the thin films.

Although the PEG molecular did not cover the entire area, the chemical reactions between the Al atoms and PEG molecules of the partially regimes were sufficient to decrease the charge injection barrier. In summary, we have found that the positive relationship between the hole numbers and electron mobility as shown in Table 4.7.

Table 4.7 The relationship between hill numbers and mobility with distinct molecular weight (M.W.) of PEG.

M. W. (g/mol)	Pure	400	1000	3000	8000	20000
Hole (numbers)	0	35	50	80	130	170
Mobility (cm ² /Vs)	0.0141	0.0245	0.0264	0.0285	0.0376	0.0440

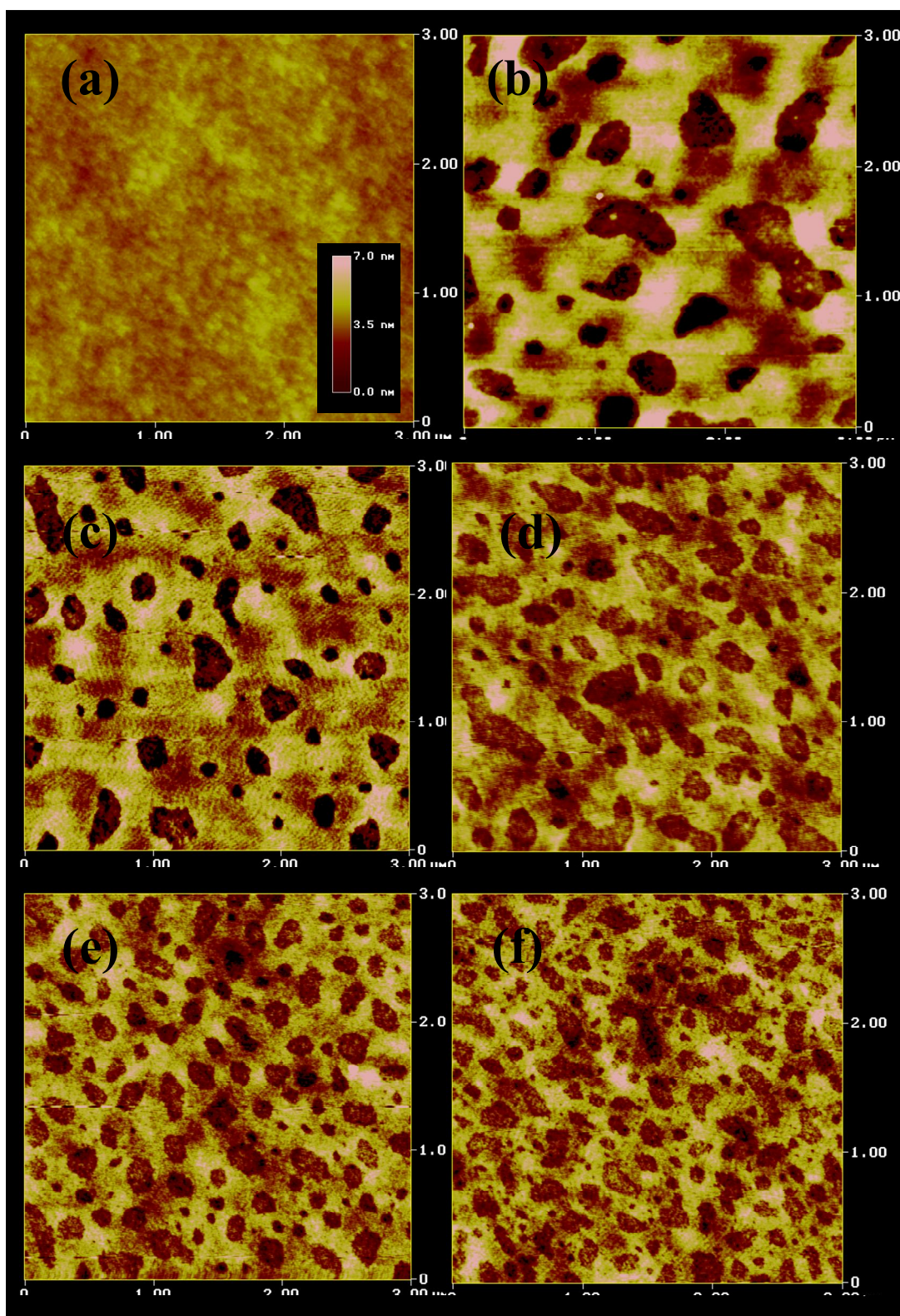


Figure 4.9 The height-mode images measured by AFM : (a) pristine PCBM, (b) to (f) PEG 400 (5%), PEG 1000 (5%), PEG 3000 (5%), PEG 8000 (5%), and PEG 20000 (5%), respectively.

4.3 Analysis of Device Resistances

The linear regime was used to extract the device resistances by transfer line method (Figure 4.10) [47]. At the linear regime, the drain bias ranged from 0 to 4 Volts for getting linear current-voltage property, and the gate bias were 30 and 60 Volts, respectively.

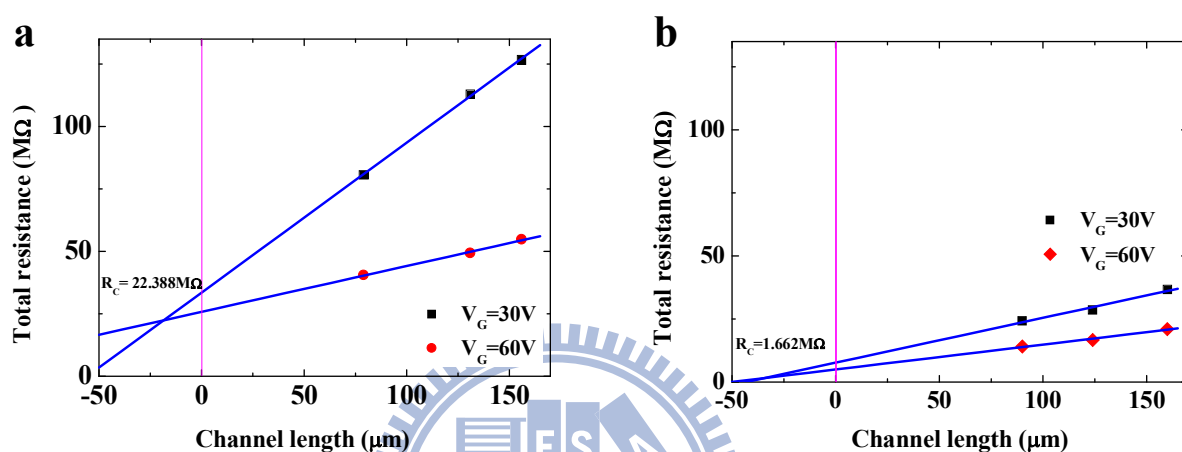


Figure 4.10 Total resistance as a function of channel resistance at various gate voltages. (a) pristine-PCBM; (b) with PEG 20000 (5%).

Table 4.8 Resistance analysis of PEG molecular weight.

PEG (g/mol)	Contact Resistance (MΩ)	Bulk Resistance (MΩ)	Parasitic Resistance (MΩ)	Channel Resistance (MΩ/μm)
Pure	22.38	3.40	25.8	0.18
400	6.22	2.77	8.99	0.08
1000	5.76	3.09	8.85	0.09
3000	5.20	2.25	7.45	0.07
8000	3.18	2.88	6.05	0.08
20000	1.66	3.31	4.98	0.09

From Figure 4.10, the parasitic resistance can be extracted by the y-axis intercept. We can separate the parasitic resistance into two parts: contact and bulk resistance. The contact resistance decreased significantly after the addition of PEG (5%) into active layer (22.4 to 1.7 M Ω). However, the bulk resistances are almost no difference in all devices (~3 M Ω). From the slope, we can extract the channel resistance. The channel resistance at $V_G=60V$ also decreased after the addition of PEG (5%) into active layer (0.18 to 0.09 M $\Omega/\mu m$). The device resistances of different PEG blended are summarized in Table 4.8.

Table 4.9 Resistance analysis of PEG blending ratio.

PEG 20000 (%)	Contact Resistance (M Ω)	Bulk Resistance (M Ω)	Parasitic Resistance (M Ω)	Channel Resistance (M $\Omega/\mu m$)
Pure	22.38	3.40	25.78	0.18
1	3.97	3.87	7.84	0.08
5	1.66	3.31	4.97	0.09
8	5.81	3.70	9.51	0.09
11	12.63	3.72	16.35	0.19
16	42.61	31.10	73.71	0.96

A low ratio of PEG present in active film (1 to 11%) can efficiently decrease the contact resistance. When 16% PEG blended into active layer, the bulk resistance increased abruptly (3.4 to 31.1 M Ω) and the channel resistance also increased (0.18 to 0.96 M Ω). The effect is attributed to the fact that too much PEG molecules would decrease the conductivity of active film. The device resistances of different PEG ratio are summarized in Table 4.9.

The decrease of the potential drop across the organic-metal interface probably change the distribution of the electric field in the vertical direction, which may influence the values of V_T .

In principle, the higher the contact resistance, the larger the V_T will be. Therefore, the decrease of contact resistance not only increased the mobility of the device, but also improved the threshold voltage. The positive relationship is shown in Table 4.1 and 4.2.

From the analysis of contact resistance, we believe that there are chemical reactions between PEG molecules and Al atoms, and these reactions may modify the contact between the metal electrodes and the active layer.



4.4 The Analysis of XPS Measurements

From Figure 4.12, we can see a main peak at a binding energy 284.5 eV. The lines with square and circular solid dots represent PCBM thin-film prepared without and with PEG 20000 (5%), respectively. The C1s spectra from 288 to 284 eV of pure PCBM/Al film is narrower than the polymer film with PEG blending due to the increasing C-O bonds. Another peak around 289.5 eV is observed in the PCBM:PEG/Al sample. The extra peak is associated with the formation of the organic oxide/Al complex [58]. We can conjecture that there are some chemical reactions between PEG and Al atoms and the interaction can decrease the charge injection barrier and also increase the injection current.

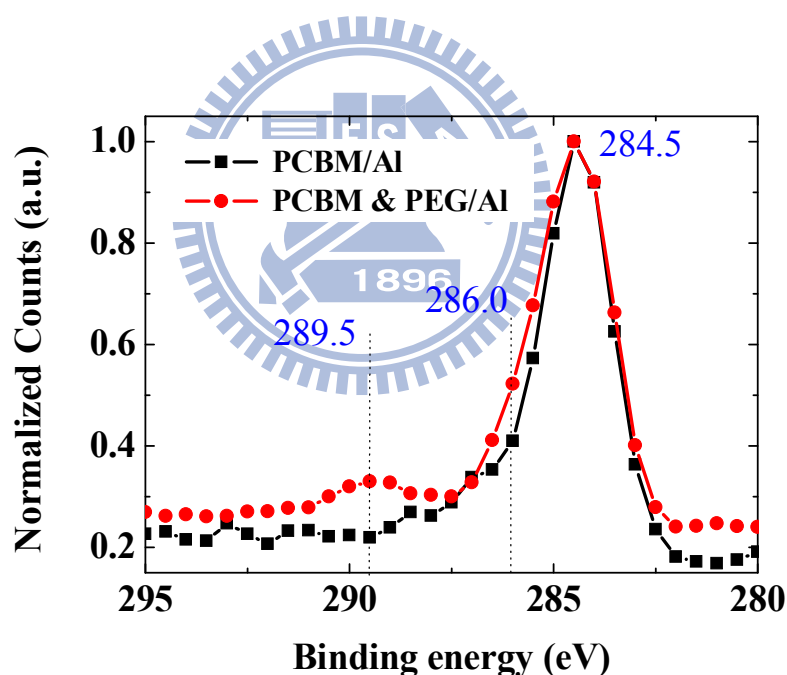


Figure 4.11 The C1s XPS spectra of PCBM/Al with and without PEG.

Chapter 5

Conclusion and Future Work

5.1 Conclusion

We have demonstrated that the mobility, threshold voltage, and on-off ratio can be improved by blending PEG into the semiconducting layer for n-channel OTFTs. We do not need another fabrication steps to modify or protect the PCBM. This enhancement was due to the injection of electron at the interface between the active layer of n-channel OTFTs and the Al S/D metal. Furthermore, the air-stability can also be improved.

We obtained the morphology information from AFM measurements. According to the relationship between the PEG molecular weight and hill numbers in the images, we infer that the phase separation in the PCBM / PEG systems occurred. We found a positive relationship between the numbers of holes and the device mobility.

The PEG molecules blended in the semiconducting layer probably underwent a chemical reaction with Al atoms. The interaction can be proved by the XPS C1s spectra. Because of that, it formed a better organic-metal contact. As a result, the contact resistance is decreased significantly after the PEG modified.

5.2 Future Work

We have demonstrated that the performance of PCBM OTFTs can be improved after the blending of PEG. With similar idea, we will further investigate the possible application of blending PEG into another n-channel semiconducting material, such as C₆₀. Solution-process C₆₀ OTFT showed the good performance, but is also difficult to fabricate. Maybe the problem could be solved in the future with this method.

Reference

1. S. R. Forrest, "The path to ubiquitous and low-cost organic electronic appliances on plastic," *Nature* **428**, 911-918 (2004).
2. F. Ebisawa, T. Kurokawa, and S. Nara, "Electrical-Properties of Polyacetylene Polysiloxane Interface," *J. Appl. Phys.* **54**, 3255-3259 (1983).
3. G. Horowitz, X. Z. Peng, D. Fichou et al., "Role of The Semiconductor Insulator Interface In The Characteristics Of Pi-Conjugated-Oligomer-Based Thin-Film Transistors," *Synth. Met.* **51**, 419-424 (1992).
4. C. D. Dimitrakopoulos and P. R. L. Malenfant, "Organic thin film transistors for large area electronics," *Adv. Mater.* **14**, 99 (2002).
5. C. R. Newman, C. D. Frisbie, D.A. da S. Filho, J. L. Bredas, P. C. Ewbank, and K. R. Mann, "Introduction to Organic Thin Film Transistors and Design of n-Channel Organic Semiconductors," *Chem. Mater.* **16**, 4436-4451 (2004).
6. A. J. Heeger, "Semiconducting and metallic polymers: the fourth generation of polymeric materials," *Synth. Met.* **125**, 23-42 (2002).
7. A. G. MacDiarmid, "A novel role for organic polymers," *Synth. Met.* **125**, 11-22 (2002).
8. G. Horowitz, "Organic field-effect transistors," *Adv. Mater.* **10**, 365 (1998).
9. P.F. Baude, D.A. Ender, M.A. Haase, T.W. Kelley, D.V. Muryres, S.D. Theiss, "Pentacene-based radio-frequency identification circuitry," *Appl. Phys. Lett.* **82**, 3964 (2002).
10. C. D. Sheraw, L. Zhou, J. R. Huang, D. J. Gundlach, T. N. Jackson, M. G. Kane, I. G. Hill, M. S. Hammond, J. Campi, B. K. Greening, J. Francl, and J. West, "Organic thin-film transistor-driven polymer-dispersed liquid crystal displays on flexible polymeric substrates," *Appl. Phys. Lett.* **80**, 1088 (2002).

11. R. Rotzoll, S. Mohapatra, V. Olariu, R. Wenz, M. Grigas, K. Dimmler, O. Shchekin, and A. Dodabalapur, "Radio frequency rectifiers based on organic thin-film transistors," *Appl. Phys. Lett.* **88**, 123502 (2006).
12. L. Zhou, A. Wanga, S. C. Wu, J. Sun, and T. N. Jackson, "All-organic active matrix flexible display," *Appl. Phys. Lett.* **88**, 083502 (2006).
13. G. H. Gelinck, H. E. A. Huitema, E. van Veenendaal, E. Cantatore, L. Schrijnemakers, J. van der Putten, T. C. T. Geuns, M. Beenhakkers, J. B. Giesbers, B. H. Huisman, E. J. Meijer, E. M. Benito, F. J. Touwslager, A. W. Marsman, B. J. E. van Rens, and D. M. de Leeuw, "Flexible active-matrix displays and shift registers based on solution-processed organic transistors," *Nat. Mater.* **3**, 106-110 (2004).
14. J. Zaumseil, and H. Sirringhaus, "Electron and Ambipolar Transport in Organic Field-Effect Transistors," *Chem. Rev.* **107**, 1296 (2007).
15. H. Klauk, M. Halik, U. Zachieschang, G. Schmid, W. Radlik, and W. Weber, "High-mobility polymer gate dielectric pentacene thin film transistors," *J. Appl. Phys.* **92**, 5259 (2002).
16. H. E. Katz, A. J. Lovinger, J. Johnson, C. Kloc, T. Siegrist, W. Li, Y. Y. Lin, and A. Dodabalapur, "A soluble and air-stable organic semiconductor with high electron mobility," *Nature* **404**, 478 (2000).
17. L. L. Chua, J. Zaumseil, J. F. Chang, E. C. W. Ou, P. K. H. Ho, H. Sirringhaus, and R. H. Friend, "General observation of n-type field-effect behaviour in organic semiconductors," *Nature* **434**, 194 (2005).
18. C. Waldauf, P. Schilinsky, M. Perisutti, J. Hauch, and C. J. Brabec, "Solution-Processed Organic n-Type Thin-Film Transistors," *Adv. Mater.* **15**, 2084-2087 (2003).
19. T. D. Anthopoulos, C. Tanase, S. Setayesh, E. J. Meijer, J. C. Hummelen, P. W. M. Blom, and D. M. de Leeuw, "Ambipolar Organic Field-Effect Transistors Based on a Solution-Processed Methanofullerene," *Adv. Mater. Weinheim, Ger.* **16**, 2174 (2004).
20. M. Chikamatsu, S. Nagamatsu, Y. Yoshida, K. Saito, and K. Yase, "Solution- Processed n-type organic thin-film transistors with high field-effect mobility," *Appl. Phys. Lett.* **87**, 203504 (2005).

21. X. Yang, J. K. J. van Duren, M. T. Rispens, J. C. Hummelen, R. A. J. Janssen, M.A.J. Michels, J. Loos, "Crystalline organization of a metha fullerene as used for plastic solar cell applications," *Adv. Mater.* **16**, 802-806, (2004)
22. S. P. Tiwari, E. B. Namdas, V. Ramgopal, D. Fichou, and S. G. Mhaisalkar, "Solution-Processed n-Type Organic Field-Effect Transistors With High ON-OFF Current Ratios Based on Fullerene Derivatives," *IEEE Device Lett.* **28**, 10 (2007).
23. P. R. L. Malenfant, C. D. Dimitrakopoulos, J. D. Gelorme, L. L. Kosbar, T. O. Graham, A. Curioni, and W. Andreoni, "N-type organic thinfilm transistor with high field-effect mobility based on a N,N8-dialkyl- 3,4,9,10-perylene tetracarboxylic diimide derivative, " *Appl. Phys. Lett.* **80**, 2517–2519 (2002).
24. T. D. Anthopoulos, B. Singh, N. Marjanovic, N. S. Sariciftci, A. M. Ramil, H. Sitter, M. Cölle, and D. M. de Leeuw, "High performance n-channel organic field-effect transistors and ring oscillators based on C60 fullerene films, " *Appl. Phys. Lett.* **89**, 213504 (2006).
25. Y. Wu, P. Liu, B. S. Ong, T. Srikumar, N. Zhao, G. Botton, and S. P. Zhu, "Controlled orientation of liquid-crystalline polythiophene semiconductors for high-performance organic thin-film transistors, " *Appl. Phys. Lett.* **86**, 142102 (2005).
26. N. Stingelin-Stutzman, E. Smits, H. Wondergem, C. Tanase, P. Blom, P. Smith, and D. de Leeuw, "Organic thin-film electronics from vitreous solution-processed rubrene hypereutectics, " *Nat. Mater.* **4**, 601–606 (2005).
27. I. McCulloh, M. Heeney, C. Bailey, K. Genovicius, I. Macdonald, M. Shkunov, D. Sparrowe, S. Tierney, R. Wagner, W. Zhang, M. L. Chabiny, R. J. Kline, M. D. McGehee, and M. F. Toney, "Liquid crystalline semiconducting polymers with high charge-carrier mobility," *Nature Mater.* **5**, 328–333 (2006).
28. A. Afzali, C. D. Dimitrakopoulos, and T. L. Breen, "High-performance, solution-processed organic thin film transistors from a novel pentacene precursor," *J. Amer. Chem. Soc.* **124**, 8812–8813 (2002).

29. T. D. Anthopoulos, D. M. de Leeuw, E. Cantatore, P. van't Hof, J. Alma, and J. C. Hummelen, "Solution processible organic transistors and circuits based on C₇₀ methanofullerene," *J. Appl. Phys.* **98**, 054503. (2005).
30. T. D. Anthopoulos, F. B. Kooistra, H. J. Wondergem, D. Kronholm, J. C. Hummelen, and D. M. de Leeuw, "Air-stable n-channel organic transistors based on a soluble C₈₄ fullerene derivative," *Adv. Mater.* **18**, 1679–1684 (2006).
31. T. B. Singh, N. Marjanovic, P. Stadler, M. Auinger, G. J. Matt, S. Günes, N. S. Sariciftci, R. Schwödiauer, and S. Bauer, "Fabrication and characterization of solution-processed methanofullerene-based organic field-effect transistors," *J. Appl. Phys.* **97**, 083714 (2005).
32. T. W. Lee, Y. Byun, B. W. Koo, I. N. Kang, Y. Y. Lyu, C. H. Lee, L. Pu, and S. Y. Lee, "All-solution-processed n-type organic transistors using a spinning metal process," *Adv. Mater.* **17**, 2180–2184 (2005).
33. L.S. Hung, C.W. Tang, M.G. Mason, "Enhanced electron injection in organic electroluminescence devices using an Al/LiF electrode," *Appl. Phys. Lett.* **70**, 152 (1997).
34. T. Hasegawa, S. Miura, T. Moriyama, T. Kimura, I. Takaya, Y. Osato, H. Mizutani, *SID Int. Symp. Dig. Tech. Papers* **35**, 154 (2004).
35. F.C. Chen, L. J. Kung, T.H. Chen, and Y.S. Lin, "Copper phthalocyanine buffer layer to enhance the charge injection in organic thin-film transistors," *Appl. Phys. Lett.* **90**, 073504 (2007).
36. J. H. Seo, A. Gutacker, B. Walker, S. Cho, A. Garcia, R. Yang, T. Q. Nguyen, A. J. Heeger, and G. C. Bazan, "Improved Injection N-Type Organic Transistors with Conjugated Poly electrolytes," *J. Am. Chem. Soc.* **131**, 18220-18221 (2009).
37. C. W. Chu, C. F. Sung, Y. Z. Lee, and K. Cheng, "Improved performance in n-channel organic thin film transistors by nanoscale interface modification," *Org. Electro.* **9**, 262-266 (2008).

38. L. L. Chua, P. K. H. Ho, H. Sirringhaus, and R. H. Friend, "Observation of Field-Effect Transistor Behavior at Self-Organized Interfaces," *Adv. Mater.* **16**, 1609-1615 (2004).
39. A. C. Arias, F. Endicott and R. A. Street, "Surface-Induced Self-Encapsulation of Polymer Thin-Film Transistors," *Adv. Mater.* **18**, 2900–2904 (2006).
40. A. Salleo, A. C. Arias, "Solution Based Self-Assembly of an Array of Polymeric Thin-Film Transistors," *Adv. Mater.* **19**, 3540-3543 (2007).
41. C. Müller, S. Goffri, D. W. Breiby, J. W. Andreasen, H. D. Chanzy, R. A. J. Janssen, M. M. Nielsen, C. P. Radano, H. Sirringhaus, P. Smith, and N. S. Stutzmann, "Tough, Semiconducting Polyethylene-poly(3-hexylthiophene) Diblock Copolymers," *Adv. Funct. Mater.* **17**, 2674–2679 (2007).
42. L. Qiu, J. A. Lim, X. Wang, W. H. Lee, M. Hwang, and K. Cho, " Versatile Use of Vertical-Phase-Separation-Induced Bilayer Structures in Organic Thin-Film Transistors," *Adv. Mater.* **20**, 1141–1145 (2008).
43. S. Y. Heriot and R. A. L. Jones, " An interfacial instability in a transient wetting layer leads to lateral phase separation in thin spin-cast polymer-blend films," *Nat. Mater.* **4**, 782-786 (2005).
44. F. C. Chen, and S. C. Chieh, "Nanoscale functional interlayers formed through spontaneous vertical separation in polymer photovoltaic devices," *J. Mater. Chem.* **19**, 6865-6869 (2009).
45. Morrison, *Organic Chemistry*, sixth edition, **502** (1992).
46. P. G. Lecomber and W. E. Spear, "Electronic Transport In Amorphous Silicon Films," *Phys. Rev. Lett.* **25**, 509 (1970).
47. P. V. Necliudov, M. S. Shur, D. J. Gundlach, and T. N. Jackson, "Contact resistance extraction in pentacene thin film transistors," *Solid-State Electro.* **47**, 259-262 (2003).

48. K. Noch, A. Elschner, J. Schwartz, A. Kahn, "Organic molecular films on gold versus conducting polymer: Influence of injection barrier height and morphology on current-voltage characteristics," *Appl. Phys. Lett.* **82**, 2281 (2003).
49. Y. Y. Lin, D. J. Gundlach, S. F. Nelson, and T. N. Jackson, "Stacked Pentacene Layer Organic Thin-Film Transistors with Improved Characteristics," *IEEE Elect. Device Let.* **18**, 606 (1997).
50. J. Takeda, M. Yamagishi, Y. Tominari, R. Hirahara, Y. Nakazaw, T. Nishikawa, T. Kawase, T. Shimoda, and S. Ogawa, "Very high-mobility organic single-crystal transistors with in-crystal conduction channels," *Appl. Phys. Lett.* **90**, 102120 (2007).
51. Y. D. Park, J. A. Lim, Y. Jang, M. Hwang, H. S. Lee, D. H. Lee, H. J. Lee, J. B. Baek, and Kilwon Cho, "Enhancement of the field-effect mobility of poly(3-hexylthiophene)/functionalized carbon nanotube hybrid transistors," *Org. Electronics*, **9**, 317-322 (2008).
52. S. Cho, J. H. Seo, K. Lee, and A. J. Heeger, "Enhanced Performance of Fullerene n-Channel Field-Effect Transistors with Titanium Sub-Oxide Injection Layer," *Adv. Funct. Mater.* **19**, 1459-1464 (2009).
53. W. Ma, C. Yang, X. Gong, K. Lee, and A. J. Heeger, "Thermally Stable, Efficient Polymer Solar Cells with Nanoscale Control of the Interpenetrating Network Morphology," *Adv. Funct. Mater.* **15**, 1617-1622 (2005).
54. G. Horowitz and P. Delannoy, "An analytical model for organic-based thin-film transistors," *J. Appl. Phys.* **70**, 469-475 (1991).
55. 陳金鑫 and 黃孝文, 有機電激發光材料與元件 (五南圖書, 2005).
56. E. V. Hauff, J. Parisi, and V. Dyakonov, "Investigation of electron injection in a methanofullerene thin film transistor," *J. Appl. Phys.* **100**, 073713 (2006).

57. D. Boudinet, G. L. Blevennec, C. Serbutoviez, J. M. Verilhac, H. Yam, and G. Horowitz, "Contact resistance and threshold voltage extraction in n-channel organic thin film transistor on plastic substrates," *J. Appl. Phys.* **105**, 084510 (2009).
58. T. F. Guo, F. S. Yang, Z. J. Tsai, T. C. Wen, S. N. Hsieh, Y. S. Fu, and C. T. Chung, "Organic oxide/Al composite cathode in effect polymer light-emitting diodes," *Appl. Phys. Lett.* **88**, 113501 (2006).

